J. Fluid Mech. (2011), *vol.* 666, *pp.* 358–390.
doi:10.1017/S0022112010004416

Transience to instability in a liquid sheet

N. S. BARLOW†, B. T. HELENBROOK AND S. P. LIN

Department of Mechanical and Aeronautical Engineering, Clarkson University, Potsdam, NY 13699-5725, USA

(Received 23 January 2010; revised 3 August 2010; accepted 4 August 2010; first published online 22 October 2010)

Series solutions are found which describe the evolution to absolute and convective instability in an inviscid liquid sheet flowing in a quiescent ambient gas and subject to a localized perturbation. These solutions are used to validate asymptotic stability predictions for sinuous and varicose disturbances. We show how recent disagreements in growth predictions stem from assumptions made when arriving at the Fourier integral response. Certain initial conditions eliminate or reduce the order of singularities in the Fourier integral. If a Gaussian perturbation is applied to both the position and velocity of a sheet when the Weber number is less than one, we observe absolutely unstable sinuous waves which grow like $t^{1/3}$. If only the position is perturbed, we find that the sheet is stable and decays like $t^{-2/3}$ at the origin. Furthermore, if both the position and velocity of a sheet are perturbed in the *absence* of ambient gas, we observe a new phenomenon in which sinuous waves neither grow nor decay and varicose waves grow like $t^{1/2}$ with a convective instability.

Key words: absolute/convective instability, capillary waves, thin films

1. Introduction

A brief history of the fluid dynamics of liquid sheets and its applications is given in Lin & Jiang (2003). Here, we mention only the work that is directly relevant to this study. As shown in the analysis of Rayleigh (1896), there are two linearly independent wave modes of a liquid sheet. The sinuous mode moves the two free surfaces of a sheet in phase. The varicose mode symmetrically moves the free surfaces in opposite directions. These modes were later confirmed in the experiments of Taylor (1959). The onset of wave instability was analysed by Squire (1953) through the use of classical temporal stability theory. The classical theory predicts, for finite $Q = \rho_g/\rho_l$ (ρ_g and ρ_l being, respectively, the gas and liquid densities), that the sinuous wave is only unstable if the Weber number is greater than one. The Weber number is defined as $We = \rho_l U^2 h_0/S$, where U is the liquid velocity in the sheet, h_0 is the half-sheet thickness and S is the interfacial tension. The experiments of Brown (1961) indicated instability for $We < 1$, which seemed to contradict the classical theory. Around this time, a new stability theory was being developed to study the complex roots of a dispersion relationship and to take into consideration the possibility of both spatial and temporal growth (Sturrock 1958). Sturrock introduced a method for determining the nature of spatio-temporal growth, and established that the mapping between frequency and wavenumber in their corresponding complex

† Email address for correspondence: barlow.nate@gmail.com

planes distinguishes whether or not an instability will convect away from its point of origin. A *convective instability* describes such a wave, while an *absolute instability* is not convected but instead grows in all directions. For an impulsively disturbed flow, Gaster (1968) showed how the asymptotic behaviour along certain rays $x/t =$ constant in the Fourier integral solution can be used to classify the instability and determine the growth rate. Gaster applied these methods to hydrodynamic flows in what came to be known as *spatio-temporal* stability theory. Bers & Briggs (1964) developed a method for determining if a flow is convectively or absolutely unstable by examining the upstream and downstream propagating branches of the dispersion relation in the complex wavenumber plane. For the case of merging upstream and downstream propagating branches, a general relationship was derived by Bers (1983) between the order of a specific singularity in the Fourier integral solution and the long-term growth rate. This method was applied by Lin, Lian & Creighton (1990) to predict neutral stability for sinuous disturbances in a liquid sheet when $We < 1$ and $Q = 0$. In the context of spatio-temporal theory, this was coined *pseudo-absolute instability* since the disturbance spreads in all directions. It was shown by De Luca & Costa (1997) that a falling (spatially developing) liquid sheet, reformulated with a slow length scale, behaves locally like a plane liquid sheet. The method of Bers (1983) was then used by De Luca & Costa (1997) to predict stable sinuous disturbances when $We > 1$ and $Q = 0$, and to predict absolutely unstable sinuous disturbances when $We < 1$ and $Q \neq 0$, which supports the findings of Brown (1961). The latter result was disputed by Luchini (2004), who derived a Fourier integral solution which predicts stable sinuous disturbances when $We < 1$ and $Q \neq 0$.

There are a few aspects of liquid sheet stability that have been endorsed across the literature (Squire 1953; Lin *et al.* 1990; De Luca & Costa 1997), namely the prediction that liquid sheets are unstable for $We > 1$ and $Q \neq 0$. This instability has since been classified as convective; the spatio-temporal analysis can be found in Lin (2003). Another point of agreement has been that varicose waves are convectively unstable for any We when $Q \neq 0$, but are stable for $Q = 0$.

In this paper, we compare series solution predictions of transient growth in a liquid sheet with classical and spatio-temporal stability predictions and develop a general procedure for finding the asymptotic growth rate. The objective of this work is to clarify the differences between the predictions of De Luca & Costa (1997) and Luchini (2004) and also to bring forth some new results. This paper is organized as follows. A description of the physical model, governing equations, and boundary conditions is given in § 2. This section also includes the Fourier integral solution method for sinuous and varicose disturbances. A review of classical and spatio-temporal stability theory is given in § 3. Briggs' method is also covered in this section, along with various interpretations of the Green's function. We develop series solutions in § 4 by solving the boundary value problems associated with sinuous and varicose waves. These solutions are evaluated in § 5 over a range of We and Q in order to examine their effect on transient wave evolution. The asymptotic analysis of the Fourier integrals is carried out in this section in order to directly compare with growth in the series solution and to determine the reasons for the various disagreements discussed above.

2. Formulation

Consider the onset to instability of an inviscid liquid sheet of uniform thickness, $2h_0$, in an inviscid ambient gas of density, ρ_g. The gas is stationary and the liquid is flowing at a constant velocity, U. At the onset of instability, the liquid flow, as well

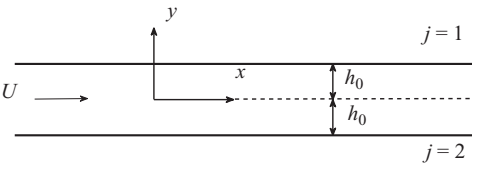

FIGURE 1. Definition sketch, a sheet with uniform thickness.

as the gas, are perturbed by two-dimensional disturbances. The fluids are assumed incompressible and the perturbed flow is assumed to be irrotational, and thus the flow potential, ϕ_j, is governed by the Laplace equation for the liquid and the gas

$$(\partial_{xx} + \partial_{yy})\phi_l = 0, \tag{2.1}$$

$$(\partial_{xx} + \partial_{yy})\phi_j = 0 \quad (j = 1, 2), \tag{2.2}$$

where (x, y) are the Cartesian coordinates in the unit of half-sheet thickness, x being the flow direction and y perpendicular to the flow. The indices $j = 1$ and 2 refer, respectively, to the gas above and below the liquid sheet (cf. figure 1).

Upon normalization of velocity by U and pressure by ρU^2, the pressure fields according to the Bernoulli equation are given by

$$p_l - p_0 = \tfrac{1}{2}[1 - (1 + \partial_x\phi_l)^2 - (\partial_y\phi_l)^2] - \partial_t\phi_l, \tag{2.3}$$

$$p_j - p_0 = -Q\left[\partial_t\phi_j + \tfrac{1}{2}(\partial_x\phi_j)^2 + \tfrac{1}{2}(\partial_y\phi_j)^2\right] \quad (j = 1, 2), \tag{2.4}$$

where p_0 is the reference pressure and t is the time normalized with h_0/U. The mean curvature of the perturbed interface is given by

$$\partial_{xx}h_j[1 + (\partial_x h_j)^2]^{-3/2} \quad (j = 1, 2), \tag{2.5}$$

where h_1 and h_2 are the distances measured in the unit of h_0 from the x-axis to the upper and lower liquid–gas interfaces, respectively.

The linearized balance of pressure difference at each interface with the surface tension force provides the linearized dynamic boundary condition

$$[Q\partial_t\phi_j - (\partial_t + \partial_x)\phi_l]_{y=(-1)^{j+1}} = (-1)^j We^{-1}\partial_{xx}h_j \quad (j = 1, 2). \tag{2.6}$$

The linearized kinematic boundary conditions are

$$[\partial_y\phi_l]_{y=(-1)^{j+1}} = (\partial_t + \partial_x)h_j, \tag{2.7}$$

$$[\partial_y\phi_j]_{y=(-1)^{j+1}} = \partial_t h_j \quad (j = 1, 2). \tag{2.8}$$

The above equations can be solved by either a Fourier series or Fourier integral approach. Here, we derive Fourier integral solutions which provide the long-time behaviour of disturbance evolution. The Fourier series solutions are later developed in § 4. We begin by Fourier transforming the dependent variables with respect to x

$$\left.\begin{aligned} &\phi_j(x, y, t) \to \hat{\phi}_j(k, y, t) \quad (j = 1, 2), \\ &\phi_l(x, y, t) \to \hat{\phi}_l(k, y, t), \\ &h_j(x, t) \to \hat{h}_j(k, t) \qquad (j = 1, 2), \end{aligned}\right\} \tag{2.9}$$

where

$$\left.\begin{aligned}\hat{h}_j(k,t) &= \int_{-\infty}^{\infty} h_j(x,t)\mathrm{e}^{-\mathrm{i}kx}\,\mathrm{d}x,\\ \hat{\phi}_j(k,y,t) &= \int_{-\infty}^{\infty} \phi_j(x,y,t)\mathrm{e}^{-\mathrm{i}kx}\,\mathrm{d}x,\\ \hat{\phi}_l(k,y,t) &= \int_{-\infty}^{\infty} \phi_l(x,y,t)\mathrm{e}^{-\mathrm{i}kx}\,\mathrm{d}x,\end{aligned}\right\} \tag{2.10}$$

and $k = k_r + \mathrm{i}k_i$ is a complex parameter. The system of equations we wish to solve is given by (2.1), (2.2), (2.6), (2.7) and (2.8). The Fourier transforms of these equations are given, respectively, as

$$(-k^2 + \partial_{yy})\hat{\phi}_l = 0, \tag{2.11}$$

$$(-k^2 + \partial_{yy})\hat{\phi}_j = 0 \quad (j = 1, 2), \tag{2.12}$$

$$[Q\partial_t\hat{\phi}_j - (\partial_t + \mathrm{i}k)\hat{\phi}_l]_{y=(-1)^{j+1}} = (-1)^{j+1}We^{-1}k^2\hat{h}_j \quad (j = 1, 2), \tag{2.13}$$

$$[\partial_y\hat{\phi}_l]_{y=(-1)^{j+1}} = (\partial_t + \mathrm{i}k)\,\hat{h}_j, \tag{2.14}$$

$$[\partial_y\hat{\phi}_j]_{y=(-1)^{j+1}} = \partial_t\hat{h}_j \quad (j = 1, 2). \tag{2.15}$$

The general solution to (2.12) contains two constants; one of which may be eliminated by applying the boundedness condition, $\hat{\phi}_j[k, (-1)^{j+1}\infty, t] = 0$, yielding

$$\hat{\phi}_j = C_g(t)\exp((-1)^j\mathrm{sgn}(k_r)ky) \quad (j = 1, 2). \tag{2.16}$$

Here, we take $\mathrm{sgn}(k_r)$ to be the generalized signum function which is undefined at $k_r = 0$. This ensures that the solution is bounded in the gas above the liquid sheet where $y > 1$ and below the liquid sheet where $y < -1$. This condition appears in various forms throughout the literature and deserves some attention. In the classical analysis of Squire (1953) and Hagerty & Shea (1955), k was a real parameter and so the $\mathrm{sgn}(k_r)k$ factor in (2.16) would have been replaced by $|k|$. In the spatio-temporal analysis of Lin *et al.* (1990), k was a complex parameter, and the analysis was carried out separately for $k_r < 0$ and $k_r > 0$. In the spatio-temporal analysis of De Luca & Costa (1997), the $\mathrm{sgn}(k_r)k$ factor was replaced by $\sqrt{k^2}$, which is only correct if the *principle* square root was taken and $k \neq 0$. As pointed out by Luchini (2004), any such factor was omitted by Lin & Jiang (2003), which invalidates their conclusions for $k_r \leqslant 0$. Here, we retain the $\mathrm{sgn}(k_r)k$ factor throughout the analysis and show that, despite this source of inaccuracy in the past, it is *not* the main cause for stability disagreements in the literature. Applying the transformed kinematic condition (2.15) to (2.16) gives

$$\hat{\phi}_j = \frac{\exp(\mathrm{sgn}(k_r)k)\partial_t\hat{h}_j}{(-1)^j\mathrm{sgn}(k_r)k}\exp((-1)^j\mathrm{sgn}(k_r)ky) \quad (j = 1, 2). \tag{2.17}$$

There are two fundamental modes in which the liquid surface may move. We shall now divide our attention between sinuous and varicose waves.

2.1. *Sinuous waves*

For the sinuous mode of solution, ϕ_l is an odd function and the two free surfaces move in unison. Applying the Fourier transformed *odd* boundary condition, $\partial_{yy}\hat{\phi}_l(k, 0, t) = 0$, to the general solution of (2.11) gives

$$\hat{\phi}_l = C_l(t)\sinh(ky). \tag{2.18}$$

Applying the transformed kinematic condition (2.14) to (2.18) gives

$$\hat{\phi}_l = \frac{(\partial_t + \mathrm{i}k)\hat{h}_j}{k\cosh(k)}\sinh(ky) \quad (j = 1, 2). \tag{2.19}$$

Substituting (2.17) and (2.19) into the transformed dynamic condition (2.13) gives a characteristic equation for $\hat{h}(k, t)$,

$$\mathrm{sgn}(k_r)Q\partial_{tt}\hat{h} + \tanh(k)(\partial_t + \mathrm{i}k)^2\hat{h} = -We^{-1}k^3\hat{h}, \tag{2.20}$$

which is identical for the top and bottom liquid surfaces. The Laplace transform of (2.20) is

$$\begin{aligned}\mathrm{sgn}(k_r)Q[-\omega^2 H(k,\omega) + \mathrm{i}\omega\hat{h}(k,0) - \partial_t\hat{h}(k,0)] + \tanh(k)\{-\omega^2 H(k,\omega) + \mathrm{i}\omega\hat{h}(k,0)\\ - \partial_t\hat{h}(k,0) + 2\mathrm{i}k[-\mathrm{i}\omega H(k,\omega) - \hat{h}(k,0)] - k^2 H(k,\omega)\} = -We^{-1}k^3 H(k,\omega),\end{aligned} \tag{2.21}$$

where

$$H(k,\omega) = \int_0^\infty \hat{h}(k,t)\mathrm{e}^{\mathrm{i}\omega t}\,\mathrm{d}t. \tag{2.22}$$

Solving for $H(k, \omega)$ in (2.21) gives

$$H(k,\omega) = \frac{[\mathrm{sgn}(k_r)Q + \tanh(k)][\mathrm{i}\omega\hat{h}(k,0) - \partial_t\hat{h}(k,0)] - 2\mathrm{i}\tanh(k)k\hat{h}(k,0)}{-\mathrm{sgn}(k_r)Q\omega^2 + \tanh(k)(-\omega^2 + 2k\omega - k^2) + We^{-1}k^3}. \tag{2.23}$$

If we take the inverse Laplace and Fourier transforms of $H(k, \omega)$, the integral solution is given by

$$h(x,t) = -\frac{1}{4\pi^2}\int_{-\infty}^{\infty}\int_{-\infty+\mathrm{i}\tau_0}^{\infty+\mathrm{i}\tau_0} H(k,\omega)\exp(\mathrm{i}(kx - \omega t))\,\mathrm{d}\omega\,\mathrm{d}k, \tag{2.24}$$

where $H(k, \omega)$ may be written as the rational expression $f(k, \omega)/D(k, \omega)$, where $f(k, \omega)$ and $D(k, \omega)$ contain no poles of k or ω. Note that the path of the ω-integral is parallel to the real axis, shifted by τ_0. This comes from the general definition of the inverse Laplace transform. The parameter τ_0 is taken such that the integration path passes above all singularities in the integrand. The dispersion relation

$$D(k,\omega) = \mathrm{sgn}(k_r)Q\omega^2 + \tanh(k)(k - \omega)^2 - We^{-1}k^3, \tag{2.25}$$

holds the significance of having ω and k roots which are singularities in (2.24). If $k_i = 0$ and $k_r > 0$, (2.25) is equivalent to the dispersion relation obtained by Squire (1953). The function $f(k, \omega)$ depends on initial conditions. When impulsively forced at a single point in space, the response $h(x, t)$ is also the Green's function $G(x, t)$ (Morse & Feshbach 1953). This interpretation is clear when the impulse is taken as a non-homogenuous term in the governing equation. However, it is convenient in stability problems, such as this, to apply the impulse through the initial conditions in the Fourier integral (2.24). We discuss this further in § 3.3. By evaluating the residues with respect to ω in (2.24), we enclose all singularities and so τ_0 in the limits of the inner Laplace integral are accounted for. The Fourier integral solution for sinuous waves is then

$$h_F(x,t) = \frac{1}{2\pi}\int_{-\infty}^{\infty}\mathrm{e}^{\mathrm{i}kx}\sum_{n=1}^{2} S_n(k)\,\mathrm{d}k, \tag{2.26}$$

where

$$S_n(k) = \mathrm{e}^{-\mathrm{i}\omega_n t}\frac{[\mathrm{sgn}(k_r)Q + \tanh(k)][\omega_n(k)\hat{h}(k,0) + \mathrm{i}\partial_t\hat{h}(k,0)] - 2k\tanh(k)\hat{h}(k,0)}{(\partial D/\partial\omega)_{\omega_n(k)}}, \tag{2.27}$$

and the two ω_n poles are given by the two ω roots of (2.25)

$$\omega_{1,2} = \frac{k}{\mathrm{sgn}(k_r)Q + \tanh(k)}\left\{\tanh(k) \pm [kWe^{-1}(\mathrm{sgn}(k_r)Q + \tanh(k)) - \mathrm{sgn}(k_r)Q\tanh(k)]^{1/2}\right\}. \tag{2.28}$$

Alternatively, the Laplace integral could have been evaluated by taking the residues with respect to k in (2.24); however, the Fourier integral is less demanding for a few reasons. The evaluation of the residues with respect to k in (2.24) is not as straightforward, since $\mathrm{sgn}(k_r)$ is not continuous along the $k_r = 0$ line. If the non-analytic point, $k_r = 0$, is ignored, the k_n poles are given by the cubic k roots of (2.25); this is done in Lin (2003). The quadratic ω roots used in the Fourier integral are far more pliant, and lead to the same asymptotic result.

2.2. *Varicose waves*

For the varicose mode of solution, ϕ_l is an even function and the two free surfaces move in opposite directions for all x. Applying the Fourier transformed *even* boundary condition, $\partial_y\hat{\phi}_l(k,0,t) = 0$, to the general solution of (2.11) gives

$$\hat{\phi}_l = C_l(t)\cosh(ky). \tag{2.29}$$

Applying the transformed kinematic condition (2.14) to (2.29) gives

$$\hat{\phi}_l = \frac{(\partial_t + \mathrm{i}k)\hat{h}_j}{(-1)^{j+1}k\sinh(k)}\cosh(ky) \quad (j = 1, 2). \tag{2.30}$$

Substituting (2.17) and (2.30) into the transformed dynamic condition (2.13) gives a characteristic equation for $\hat{h}(k,t)$

$$\mathrm{sgn}(k_r)Q\partial_{tt}\hat{h} + \coth(k)(\partial_t + \mathrm{i}k)^2\hat{h} = -We^{-1}k^3\hat{h}, \tag{2.31}$$

which is identical for the top and bottom liquid surfaces. The only difference between (2.20) and (2.31) is that $\tanh(k)$ has been replaced by $\coth(k)$. The derivation then is identical to that of the sinuous case, except for the eventual removal of the $\coth(k)$ function so that $f(k,\omega)$ and $D(k,\omega)$ contain no singularities. The dispersion relation and Fourier integral solution for varicose waves are given, respectively, by

$$D(k,\omega) = \sinh(k)\mathrm{sgn}(k_r)Q\omega^2 + \cosh(k)(k-\omega)^2 - \sinh(k)We^{-1}k^3 \tag{2.32}$$

and

$$h_F(x,t) = \frac{1}{2\pi}\int_{-\infty}^{\infty}\mathrm{e}^{\mathrm{i}kx}\sum_{n=1}^{2}V_n(k)\,\mathrm{d}k, \tag{2.33}$$

where

$$V_n(k) = \mathrm{e}^{-\mathrm{i}\omega_n t}\frac{[\sinh(k)\mathrm{sgn}(k_r)Q + \cosh(k)][\omega_n(k)\hat{h}(k,0) + \mathrm{i}\partial_t\hat{h}(k,0)] - 2k\cosh(k)\hat{h}(k,0)}{(\partial D/\partial\omega)_{\omega_n(k)}}, \tag{2.34}$$

Wave	Q	We	Instability/growth
Either	$=0$	Any	Neutral
Sinuous	$\neq 0$	<1	Neutral
Sinuous	$\neq 0$	>1	Unstable, $\exp(\max(\omega_i)t)$
Varicose	$\neq 0$	any	Unstable, $\exp(\max(\omega_i)t)$

TABLE 1. Classical temporal stability predictions for sinuous and varicose waves.

and the two ω_n poles are given by the ω roots of (2.32)

$$\omega_{1,2} = \frac{k}{\sinh(k)\mathrm{sgn}(k_r)Q + \cosh(k)} \left\{\cosh(k) \pm [k\sinh(k)We^{-1}(\sinh(k)\mathrm{sgn}(k_r)Q + \cosh(k)) - \sinh(k)\mathrm{sgn}(k_r)Q\cosh(k)]^{1/2}\right\}. \quad (2.35)$$

3. Stability analysis

Here we review the classical temporal stability theory for liquid sheets and outline spatio-temporal theory in general.

3.1. *Classical temporal predictions*

In classical stability theory, the solution can be thought of as a superposition of modes, each given by $A_k \exp(\mathrm{i}(kx - \omega t))$, where A_k is the amplitude associated with a particular mode. Here, k is a real parameter and $\omega = \omega_r + \mathrm{i}\omega_i$ is the complex wave frequency. A positive ω_i value leads to exponential growth in time; if $\omega_i > 0$, the solution is temporally *unstable*. The temporal growth rate, ω_i, is evaluated from the ω roots of the dispersion relation, given for sinuous waves in (2.28) and for varicose waves in (2.35). It can be shown that ω_i is zero for all k when $Q = 0$ for both types of waves. Thus the sheet is predicted to be neutrally stable for any We in the absence of ambient gas. It can also be shown for long sinuous waves (small k) and finite Q, that $\omega_i \neq 0$ for $We > 1$, and $\omega_i = 0$ for $We < 1$. This led to the conclusion of Squire (1953) that sinuous waves in a liquid sheet can only become unstable for $We > 1$. For long varicose waves and finite Q, the classical theory predicts instability for any We. A detailed review of the classical analysis can be found in Lin (2003). The classical stability predictions are listed in table 1 for reference.

Unstable waves grow at the rate $\exp(\max(\omega_i)t)$, where $\max(\omega_i)$ is determined by plotting the branches of either (2.28) or (2.35). These *temporal amplification plots* are shown in figure 2 for both sinuous and varicose waves. The maximum growth rates are indicated on each plot. In § 5, these rates are compared with growth in the series solution. As shown in figures 2(*a*) and 2(*c*), the growth rate is greater for sinuous waves than for varicose waves. For this reason, sinuous waves have been considered the dominant mode for breakup when $Q \neq 0$. A few limitations of classical theory are that only exponential growth is considered and the *type* of growth is not predicted. In § 3.2, we review absolute and convective instability. In § 5, we show how algebraic growth may also be predicted.

If we make the long-wave approximation ($k \to 0$), it can be shown for $Q = 0$ that the group velocity is $\mathrm{d}\omega_r/\mathrm{d}k_r = 1 \pm We^{-1/2}$ for sinuous waves and $\mathrm{d}\omega_r/\mathrm{d}k_r = 1 \pm 2We^{-1/2}k$ for varicose waves. For $We > 1$, a sinuous disturbance splits into two downstream propagating packets. For $We < 1$, a sinuous disturbance splits into one downstream propagating packet and one upstream propagating packet. By including the ambient

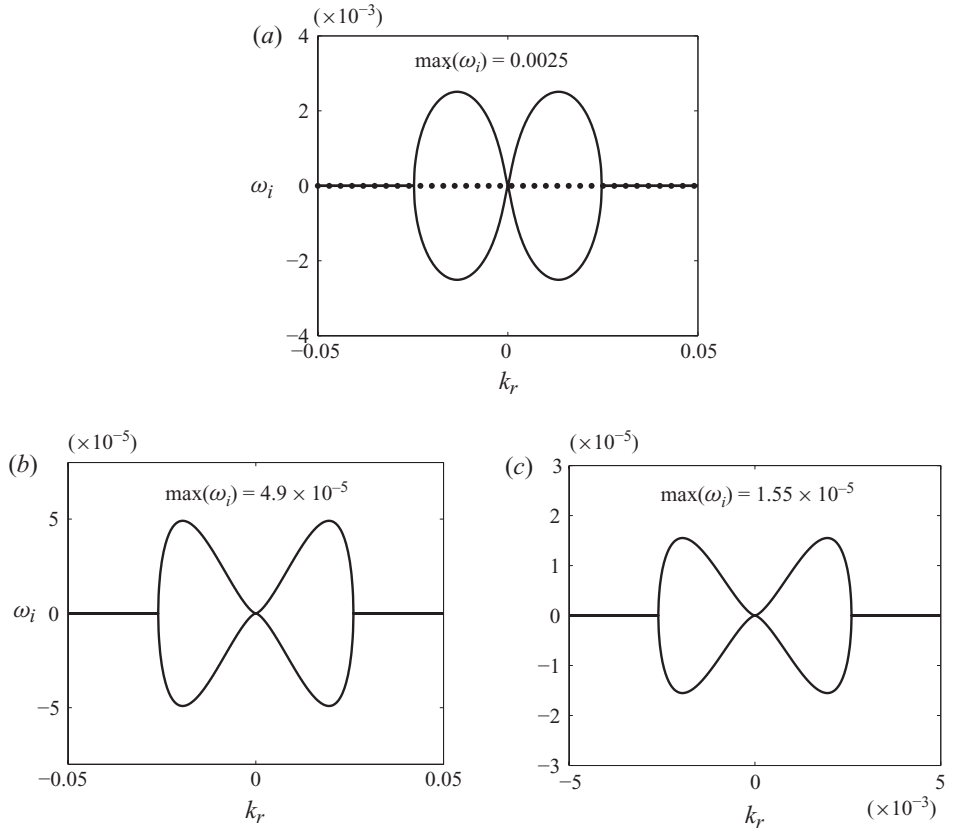

FIGURE 2. (*a*) Temporal amplification curves for sinuous waves given by (2.28): $Q = 0.0013$, $We = 20$ (——); $Q = 0.13$, $We = 0.02$ (●). Temporal amplification curves for varicose waves given by (2.35): (*b*) $Q = 0.0013$, $We = 20$; (*c*) $Q = 0.13$, $We = 0.02$.

gas ($Q \neq 0$), the group velocity of sinuous waves is altered, but the propagation directions are preserved. This can be seen when comparing the ω_r versus k_r slopes in figure 3(*a*,*b*) for $Q = 0$ (——) and $Q \neq 0$ (– –). These plots are obtained directly from (2.28), where a long-wave approximation has not been made. For $We < 1$(figure 3*b*), upstream and downstream waves are present for all k_rs if $Q = 0$, indicated by the positive and negative slopes. For $We > 1$ (figure 3*a*), two downstream waves are present for all k_rs if $Q = 0$. However, for $We > 1$ and $Q \neq 0$, it can be seen that the branches converge to a single group velocity over a specific k_r range; this is the same range of k_r responsible for growth, as indicated in figure 2. This can also be confirmed for varicose waves in figure 3(*c*,*d*). This indicates that exponentially growing disturbances travel at a single group velocity.

3.2. *Review of spatio-temporal stability theory*

In general, there are three stability states for a propagating wave, defined by the long-time behaviour of (2.24). Here, we take the wave to be initiated by an impulsive disturbance. As $t \to \infty$, neutrally stable, stable and unstable waves are, respectively, defined by $\|G(x,t)\|_\infty = \text{constant}$, $\|G(x,t)\|_\infty \to 0$ and $\|G(x,t)\|_\infty \to \infty$ where the norm is the L_∞ norm, which is the maximum of the function over x. If a wave is either neutral or unstable, the long time behaviour can be further classified as

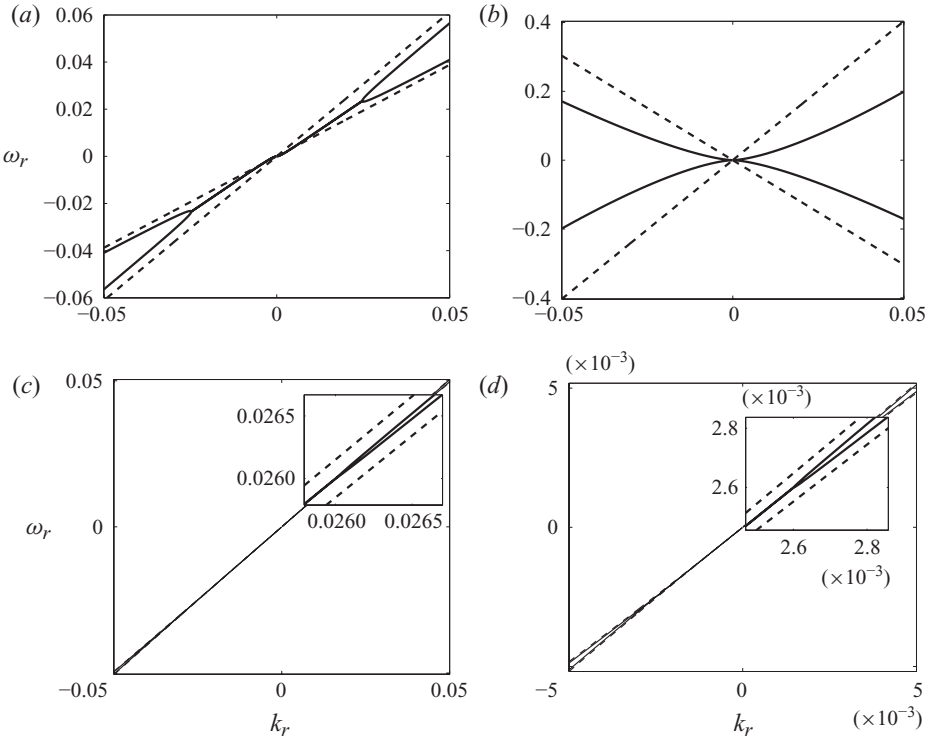

FIGURE 3. Propagation curves for sinuous waves (a, b) given by (2.28) and varicose waves (c,d) given by (2.35) . (a, c) $We = 20$ and $Q = 0.0013$ (——), $Q = 0$ (— —); (b, d) $We = 0.02$ and $Q = 0.13$ (——), $Q = 0$ (— —).

convective if $G(x = 0, t) \to 0$ or *absolute* if $G(x = 0, t) \to \infty$ as $t \to \infty$ (Bers & Briggs 1964). While these provide general definitions for instability, it is convenient to treat the disturbance as a wavepacket and examine the growth along specific rays $x/t =$ constant when evaluating the Fourier integrals in § 5. To this end, we build upon the definitions of Huerre & Monkewitz (1990). A sufficient condition for neutral stability is that

$$G(x, t) \text{ is non-vanishing along at least one ray } \frac{x}{t} = \text{constant}$$
$$\text{and there are no rays upon which } G(x, t) \text{ is growing.} \quad (3.1)$$

If the response to an impulse disturbance decays in time for all x, it is considered a *linearly stable* travelling wave. The long-time behaviour is given by

$$\lim_{t\to\infty} G(x, t) = 0 \text{ along all rays } \frac{x}{t} = \text{constant.} \quad (3.2)$$

If the response grows in time, it is considered a *linearly unstable* travelling wave, given by

$$\lim_{t\to\infty} G(x, t) \to \infty \text{ along at least one ray } \frac{x}{t} = \text{constant.} \quad (3.3)$$

Once the response has been classified as unstable, the type of instability may also be determined. If the disturbance grows but is convected away from the location of the

initial impulse, the long-time behaviour is also given by

$$\lim_{t\to\infty} G(x,t) = 0 \text{ along the ray } \frac{x}{t} = 0. \tag{3.4}$$

Limits (3.3) and (3.4) together describe a *convectively unstable* wave, while limits (3.1) and (3.4) describe a *convectively neutral* wave. If the disturbance grows but is not convected away from its origin, the long-time behaviour is given by

$$\lim_{t\to\infty} G(x,t) \to \infty \text{ along the ray } \frac{x}{t} = 0, \tag{3.5}$$

which defines an *absolutely unstable* wave. An *absolutely neutral* wave, also described as *pseudo-absolute instability* (Lin *et al.* 1990), is defined by (3.1) and

$$\lim_{t\to\infty} G(x,t) \text{ is non-vanishing along the ray } \frac{x}{t} = 0. \tag{3.6}$$

An alternative way of viewing the instability is through a *spatial amplification plot*, where the ω_i contours of $D(k,\omega)$ are plotted over the k_i–k_r plane. Along isocontours of ω_i, each wavenumber, k_r, is associated with a spatial growth rate, k_i. The $\omega_i > 0$ isocontours represents unstable modes which grow exponentially in time. The $\omega_i = 0$ isocontour represents modes which do not grow exponentially, and so instability arises only if these modes grow algebraically in time, as determined by the Fourier integral. For $t > 0$, the $\omega_i < 0$ contours represent decaying modes, which do not lead to instability. One can determine whether the instability is convective or absolute by separately examining the downstream (or upstream) propagating ω_i isocontours in the k_i–k_r plane as they approach $\omega_i = 0$. This is equivalent to lowering the ω integration path in (2.24), by decreasing τ_0. We use this process, known as Briggs' method, in § 5 to support the asymptotic analysis. A detailed explanation of this method can be found in Briggs (1964), Bers (1983) and Huerre & Monkewitz (1990). Some pedagogic examples are given in Huerre (1987), Schmid & Henningson (2001) and Barlow *et al.* (2010).

3.3. *Response to impulsive initial conditions*

The Fourier integral solution is still a general solution, as it is subject to the choice of initial conditions $h(x,0)$ and $\partial_t h(x,0)$. A clear choice for an impulse response is $h(x,0) = \delta(x)$. A source of disparity in the literature stems from the veiled and perhaps involuntary choice for the initial disturbance velocity, $\partial_t h(x,0)$. Here, we examine the response to the conditions $h(x,0) = \delta(x)$ and $\partial_t h(x,0) = 0$ and designate the solution as $G_{stat}(x,t)$, the *static Green's function*. We designate the actual Green's function, $G(x,t)$, as the response to $h(x,0) = \partial_t h(x,0) = \delta(x)$. This coincides with the impulse response of a second-order system, physically interpreted as a jump in velocity and position at $t = 0$. Another choice for the initial disturbance velocity can be obtained by setting the initial vertical velocity along the liquid interface ($[\partial_y \phi_l]_{y=(-1)^{j+1}}$) to zero, reducing the kinematic condition (2.7) to $\partial_t h(x,0) = -\partial_x h(x,0)$. This causes symmetric wave propagation and was used in Lin (2003) to clearly show the upstream and downstream propagating waves for $We < 1$ and $Q = 0$. We designate the solution to these conditions as $G_{sym}(x,t)$, the *symmetric response*. The Fourier transformed responses are given in table 2 so that we may later apply them to the Fourier integral solution.

Response	$\hat{h}(k,0)$	$\partial_t\hat{h}(k,0)$
G_{stat}	1	0
G	1	1
G_{sym}	1	$-\mathrm{i}k$

TABLE 2. Types of initial conditions to be examined.

4. Series solutions

We find series solutions for sinuous and varicose waves using a collection of spatial modes. This is done to compare the behaviour of a disturbance defined on a bounded domain with growth predictions of the Fourier integral solution, which is defined on an unbounded domain. We utilize the method developed by Barlow *et al.* (2010) in order to represent solutions using any horizontal line in the complex k_i–k_r plane. The analysis of these solutions is then given in § 5, where we compare the disturbance growth rates with the classical and asymptotic predictions.

We wish to solve (2.1) and (2.2) as boundary value problems. To carry out the separation of variables for the gas phase, we assume the form $\phi_j(x,y,t) = X(x,t)Y(y,t)$, which transforms (2.2) into

$$\frac{Y''(y,t)}{Y(y,t)} = -\frac{X''(x,t)}{X(x,t)} = k^2, \tag{4.1}$$

where the complex separation constant is given by $k = k_r + \mathrm{i}k_i$. The boundary conditions for $\phi_j(x,y,t)$ are given by

$$\left.\begin{aligned} \phi_j(L,y,t) &= B\phi_j(0,y,t), \\ \partial_x\phi_j(L,y,t) &= B\partial_x\phi_j(0,y,t) \end{aligned}\right\} \tag{4.2}$$

and

$$\phi_j[x,(-1)^{j+1}\infty,t] = 0 \quad \text{(bounded in } y\text{)}, \tag{4.3}$$

where L is the domain length and B is a real parameter representing the jump in magnitude of the solution across the boundary. For $B = 1$, the domain is periodic. For $B \neq 1$, the domain is *jump periodic*. Jump-periodic boundary conditions allow for spatially growing or decaying modes in the solution. If the disturbance width is taken to be much smaller than L, the boundary conditions should be inconsequential to disturbance growth. As long as there is a quiescent region between the disturbance and the boundaries, we should be able to compare with impulse response growth predictions. For X, we have the ordinary differential equation, $X'' + k^2X = 0$ with the general solution, $X(x,t) = C_1(t)\cos(kx) + C_2(t)\sin(kx)$. Applying boundary conditions (4.2) leads to a non-trivial solution if $\cos(k_r)\cosh(k_i) = 1/2B + B/2$ and $\sinh(k_i)\sin(k_r) = 0$. Hence, k_r is the wavenumber defined by

$$k_{r,n} = 2n\pi, \quad n = 0, \pm1, \pm2, \ldots \tag{4.4}$$

and $k_i = \cosh^{-1}(1/2B + B/2)$ is the spatial growth at the boundary. Thus, by choosing different values of B, we are essentially using modes with complex wavenumbers taken from the horizontal line $k_i = \cosh^{-1}(1/2B + B/2)$ in the complex plane. For $Y_n(y,t)$, we have the ordinary differential equation, $Y_n'' - k_n^2Y_n = 0$. The general solution can be written like $Y_n = C_{3n}(t)\mathrm{e}^{k_n y} + C_{4n}(t)\mathrm{e}^{-k_n y}$. Applying the boundedness condition (4.3) reduces this to $Y_n = C_n(t)\exp((-1)^j\mathrm{sgn}(k_{r,n})k_n y)$. If we also cast $X(x,t)$ in complex

exponential form, the general solution, $\phi_j(x, y, t) = X(x, t)Y(y, t)$, can be written with a single constant, $C_{g,n}(t)$, per mode as

$$\phi_j(x, y, t) = \sum_{n=-N/2}^{N/2} C_{g,n}(t) \exp(\mathrm{i}k_n x) \exp((-1)^j \operatorname{sgn}(k_{r,n}) k_n y) \quad (j = 1, 2), \tag{4.5}$$

where N is the number of modes chosen to represent the solution and $k_n = k_{r,n} + k_i$. Applying the kinematic condition (2.8) to a single mode of (4.5) gives

$$\phi_{j,n}(x, y, t) = \frac{\exp(\operatorname{sgn}(k_{r,n})k)\partial_t h_{j,n}}{(-1)^j \operatorname{sgn}(k_{r,n}) k_n} \exp((-1)^j \operatorname{sgn}(k_{r,n}) k_n y) \quad (j = 1, 2), \tag{4.6}$$

which matches its Fourier transformed counterpart (2.17). To carry out the separation of variables for the liquid phase, we assume the form $\phi_l(x, y, t) = X(x, t)Y(y, t)$ and apply the jump-periodic conditions

$$\left.\begin{aligned} \phi_l(L, y, t) &= B\phi_l(0, y, t), \\ \partial_x \phi_l(L, y, t) &= B\partial_x \phi_l(0, y, t). \end{aligned}\right\} \tag{4.7}$$

We also apply odd and even boundary conditions

$$\left.\begin{aligned} \partial_{yy}\phi_l(x, 0, t) &= 0, \\ \partial_y \phi_l(x, 0, t) &= 0, \end{aligned}\right\} \tag{4.8}$$

used, respectively, for sinuous and varicose motions along the liquid interfaces. The solution for $\phi_l(x, y, t) = X(x, t)Y(y, t)$ is then

$$\phi_l(x, y, t) = \sum_{n=-N/2}^{N/2} C_{l,n}(t) \mathrm{e}^{\mathrm{i}k_n x} \sinh(k_n y), \tag{4.9}$$

for the sinuous mode and

$$\phi_l(x, y, t) = \sum_{n=-N/2}^{N/2} C_{l,n}(t) \mathrm{e}^{\mathrm{i}k_n x} \cosh(k_n y), \tag{4.10}$$

for the varicose mode. Applying the kinematic condition (2.7) to a single mode of (4.9) and (4.10) gives

$$\phi_{l,n}(x, y, t) = \frac{(\partial_t + \partial_x) h_{j,n}}{k_n \cosh(k_n)} \sinh(k_n y) \quad (j = 1, 2), \tag{4.11}$$

for the sinuous mode and

$$\phi_{l,n}(x, y, t) = \frac{(\partial_t + \partial_x) h_{j,n}}{(-1)^{j+1} k_n \sinh(k_n)} \cosh(k_n y) \quad (j = 1, 2), \tag{4.12}$$

for the varicose mode. If we take the solution form for interface displacement to be

$$h_j(x, t) = \sum_{n=-N/2}^{N/2} C_{h,n}(t) \mathrm{e}^{\mathrm{i}k_n x} \quad (j = 1, 2), \tag{4.13}$$

and substitute (4.6) and (4.11)/(4.12) into the dynamic condition (2.6), we obtain the ordinary differential equation

$$a_{s/v,n} \frac{\mathrm{d}^2 C_{h,n}}{\mathrm{d}t^2} + b_{s/v,n} \frac{\mathrm{d}C_{h,n}}{\mathrm{d}t} + c_{s/v,n} C_{h,n} = 0, \tag{4.14}$$

which is identical for the top and bottom liquid surfaces. The coefficients for sinuous waves are given by

$$a_{s,n} = \mathrm{sgn}(k_{r,n})Q + \tanh(k_n), \tag{4.15}$$
$$b_{s,n} = 2\mathrm{i}k\tanh(k_n), \tag{4.16}$$
$$c_{s,n} = -k^2\tanh(k_n) + We^{-1}k_n^3, \tag{4.17}$$

and the coefficients for varicose waves are given by

$$a_{v,n} = \mathrm{sgn}(k_{r,n})Q\sinh(k_n) + \cosh(k_n), \tag{4.18}$$
$$b_{v,n} = 2\mathrm{i}k\cosh(k_n), \tag{4.19}$$
$$c_{v,n} = -k^2\cosh(k_n) + We^{-1}k_n^3\sinh(k_n). \tag{4.20}$$

The solution to (4.14) is then given by

$$h(x,t) = \sum_{|n|<N/2}\left[\left(C_{h1,n}\mathrm{e}^{r_{+,n}t} + C_{h2,n}\mathrm{e}^{r_{-,n}t}\right)\mathrm{e}^{\mathrm{i}k_n x}\right] + \left[C_{h1,0} + tC_{h2,0}\right]_{n=0}, \tag{4.21}$$

where $r_{\pm,n} = (-b_{s,n} \pm \sqrt{b_{s,n}^2 - 4a_{s,n}c_{s,n}})/(2a_{s,n}) \neq 0$ for sinuous waves and $r_{\pm,n} = (-b_{v,n} \pm \sqrt{b_{v,n}^2 - 4a_{v,n}c_{v,n}})/(2a_{v,n}) \neq 0$ for varicose waves. The first term in (4.21) corresponds with all distinct roots, while the second term corresponds with the double root at $k = r_{\pm,n} = 0$. For $t = 0$, (4.21) is the complex Fourier series (as $N \to \infty$) and the coefficients are obtained by solving

$$\left.\begin{aligned} C_{h1,n\neq0} + C_{h2,n\neq0} = C_{h1,0} &= \frac{1}{L}\int_0^L h_0(x)\,\mathrm{e}^{-\mathrm{i}k_{r,n}x}\,\mathrm{d}x, \\ r_{+,n}C_{h1,n\neq0} + r_{-,n}C_{h2,n\neq0} = C_{h2,0} &= \frac{1}{L}\int_0^L [\partial_t h]_{t=0}(x)\,\mathrm{e}^{-\mathrm{i}k_{r,n}x}\,\mathrm{d}x, \end{aligned}\right\} \tag{4.22}$$

where $h_0(x)$ is the initial disturbance shape and $[\partial_t h]_{t=0}(x)$ is the initial disturbance velocity. The initial impulsive disturbance is approximated by a Gaussian centred at $x = 0$ and given by

$$h_0(x) = h_\delta(x) = 0.1\exp(-x^2/100), \tag{4.23}$$

which is an order of magnitude wider than the unit sheet thickness and thus a reasonable approximation for long waves on thin sheet. The initial disturbance velocity is approximated by either

$$\left.\begin{aligned} [\partial_t h]_{t=0}(x) &= 0, \\ [\partial_t h]_{t=0}(x) &= h_\delta(x), \\ [\partial_t h]_{t=0}(x) &= -\frac{\mathrm{d}h_0}{\mathrm{d}x}, \end{aligned}\right\} \tag{4.24}$$

or

in order to simulate the responses $G_{stat}(x,t)$, $G(x,t)$ and $G(x,t)_{sym}$ described in § 3.3. For the analysis shown in § 5, we let $k_i = 0$ ($B = 1$), meaning that we have a purely periodic domain. For $k_i \neq 0$, we previously showed (Barlow *et al.* 2010) that the solutions are identical for any k_i as long as the perturbation does not reach the boundary.

5. Asymptotic predictions and transient solutions

We shall now find the asymptotic ($t \to \infty$) behaviour of the Fourer integrals (2.26) and (2.33), which describe sinuous and varicose waves, and compare it with the series solutions constructed using (4.21). When $Q = 0$, the Fourier integrals can be simplified and the analysis becomes clearer. In § 5.1, we take advantage of this and illustrate the details of the asymptotic method, which is then applied for $Q \neq 0$ in § 5.2.

5.1. *Absence of ambient gas ($Q = 0$)*

The classical theory predicts stable waves for both sinuous and varicose disturbances in the absence of ambient gas (Squire 1953; Hagerty & Shea 1955). Using asymptotic analysis, Lin *et al.* (1990) also determined that sinuous waves are stable for $We < 1$, but predicted that they are neutrally stable for $We > 1$. In the aforementioned works, the long-wavelength approximation was not used, and so these predictions generalize to thin and thick sheets. In the present work, we apply asymptotic analysis to show that, for $Q = 0$ and *any* We, long sinuous waves are convectively neutral. Although the long-wave approximation is used to obtain the stability results, the predictions agree well with the series solutions presented here, where no such approximation is used.

It has been stated by Lin *et al.* (1990) and De Luca & Costa (1997) that varicose waves are stable for any We in the absence of ambient gas. Here, we show how varicose waves in the absence of ambient gas become algebraically convectively unstable when subjected to an impulsive initial disturbance velocity.

For long waves (small k) we let $\sinh(k) \to k$ and $\cosh(k) \to 1$. By letting $Q = 0$, the sinuous (2.25) and varicose (2.32) dispersion relations reduce to

$$D(k, \omega) = k\,(k - \omega)^2 - We^{-1}k^3 \tag{5.1}$$

and

$$D(k, \omega) = (k - \omega)^2 - We^{-1}k^4, \tag{5.2}$$

and the $\pm$ branches of the sinuous (2.26) and varicose (2.33) Fourier integrals reduce to

$$h_{\pm}(x, t) = \frac{1}{2\pi}\int_{-\infty}^{\infty} \frac{\hat{h}(k, 0)k[\omega_{\pm}(k) - 2k] + \mathrm{i}k\partial_t\hat{h}(k, 0)}{(\partial D/\partial\omega)_{\omega_{\pm}(k)}} \mathrm{e}^{\psi(k)t}\,\mathrm{d}k \tag{5.3}$$

and

$$h_{\pm}(x, t) = \frac{1}{2\pi}\int_{-\infty}^{\infty} \frac{\hat{h}(k, 0)[\omega_{\pm}(k) - 2k] + \mathrm{i}\partial_t\hat{h}(k, 0)}{(\partial D/\partial\omega)_{\omega_{\pm}(k)}} \mathrm{e}^{\psi(k)t}\,\mathrm{d}k, \tag{5.4}$$

where $\omega_{\pm}(k) = k \pm kWe^{-1/2}$ for long sinuous waves, $\omega_{\pm}(k) = k \pm k^2We^{-1/2}$ for long varicose waves and $\psi(k) = \mathrm{i}[k(x/t) - \omega_{\pm}(k)]$ is the phase.

We shall first examine long sinuous waves. In the absence of ambient gas, a sinuous wavepacket moves at a group velocity of $\mathrm{d}\omega_r/\mathrm{d}k_r = 1 \pm We^{-1/2}$. The phases which correspond to $x/t = 0$ and $x/t = 1 \pm We^{-1/2}$ are $\psi(k) = -\mathrm{i}k(1 \pm We^{-1/2})$ and $\psi(k) = 0$. After evaluating (5.3) along these rays, we obtain

$$\begin{aligned}[h(t)]_{x/t=0} = {} & \frac{1}{4\pi}\int_{-\infty}^{\infty} \hat{h}(k, 0)[\exp(-\mathrm{i}k(1 + We^{-1/2})t) + \exp(-\mathrm{i}k(1 - We^{-1/2})t)]\,\mathrm{d}k \\ & + \frac{\mathrm{i}We^{1/2}}{4\pi}\int_{-\infty}^{\infty} \frac{\partial_t\hat{h}(k, 0)}{k}[\exp(-\mathrm{i}k(1+We^{-1/2})t) - \exp(-\mathrm{i}k(1-We^{-1/2})t)]\,\mathrm{d}k\end{aligned} \tag{5.5}$$

and

$$[h(t)]_{x/t=1\pm We^{-1/2}} = \frac{1}{2\pi}\int_{-\infty}^{\infty} \hat{h}(k,0)\,\mathrm{d}k = [h_0(x)]_{x=0}, \tag{5.6}$$

where

$$h_0(\xi) = \frac{1}{2\pi}\int_{-\infty}^{\infty} \hat{h}(k,0)\mathrm{e}^{-k\xi}\,\mathrm{d}k \tag{5.7}$$

is the initial disturbance. The variable ξ generalizes (5.7) for further use. Since there is no time dependence in (5.6), the response along $x/t = 1 \pm We^{-1/2}$ is given by

$$G(x,t) = G_{stat}(x,t) = G_{sym}(x,t) = \text{constant} \tag{5.8}$$

for any initial condition. If we subject (5.5) to the initial conditions in table 2 and make use of (5.7), the responses along $x/t = 0$ become

$$\left.\begin{aligned} G_{stat}(x,t) &= \frac{1}{2}\delta[-(1+We^{-1/2})t] + \frac{1}{2}\delta[-(1-We^{-1/2})t], \\ G_{sym}(x,t) &= \left(\frac{1}{2} + \frac{We^{-1/2}}{4\pi}\right)\delta[-(1+We^{-1/2})t] + \left(\frac{1}{2} + \frac{We^{-1/2}}{4\pi}\right) \\ &\quad \times \delta[-(1-We^{-1/2})t], \end{aligned}\right\} \tag{5.9}$$

and

$$G(x,t) = \frac{1}{2}\delta[-(1+We^{-1/2})t] + \frac{1}{2}\delta[-(1-We^{-1/2})t] + \frac{We^{1/2}}{2\pi}\int_0^{\infty} \frac{\sin[k(1-We^{-1/2})t] - \sin[k(1+We^{-1/2})t]}{k}\,\mathrm{d}k, \tag{5.10}$$

where $h_0(\xi)$ has been replaced by the delta function $\delta(\xi) = (1/2\pi)\int_{-\infty}^{\infty}\mathrm{e}^{-kx}\,\mathrm{d}k$, which is zero for $\xi \neq 0$. Also, Euler's identity and even/odd relations have been applied to the integral in (5.10) in order to make use of the relation $\int_0^{\infty}(\sin(\beta k)/k)\,\mathrm{d}k = (\pi/2)\mathrm{sgn}(\beta)$ (Seeley 1966). The long-time responses along $x/t = 0$ now become

and

$$\left.\begin{aligned} &\lim_{t\to\infty} G_{stat}(x,t) = \lim_{t\to\infty} G_{sym}(x,t) = 0 \\ &\lim_{t\to\infty} G(x,t) = \begin{cases} 0 & \text{if } We > 1, \\ \text{constant} & \text{if } We < 1. \end{cases} \end{aligned}\right\} \tag{5.11}$$

By definitions (3.1) and (3.4), (5.8) and (5.11) predict that the response $G(x,t)$ is convectively neutral for $We > 1$ and the responses G_{stat} and G_{sym} are convectively neutral for any Weber number. This differs from the analysis of De Luca & Costa (1997) and Lin (2003), where *stable* sinuous waves are predicted for $We > 1$. By definitions (3.1) and (3.6), the response $G(x,t)$ predicts absolutely neutral waves for $We < 1$, which agrees with the analysis of Lin *et al.* (1990).

For the remaining Green's functions obtained in this section, it is useful to have an approximation for infinite and semi-infinite integrals which lead to algebraic growth, such as

$$I(k,t) = \int_C \frac{\mathrm{e}^{\gamma k^m t}}{k^s}\,\mathrm{d}k \approx t^{(s-1)/m}, \quad m \neq 0, \tag{5.12}$$

where γ is some constant. This result can be shown for $s < 1$ using the gamma function, where $\int_C$ is $\int_0^{\infty}$ (Bender & Orszag 1978). If there is symmetry about $k_r = 0$,

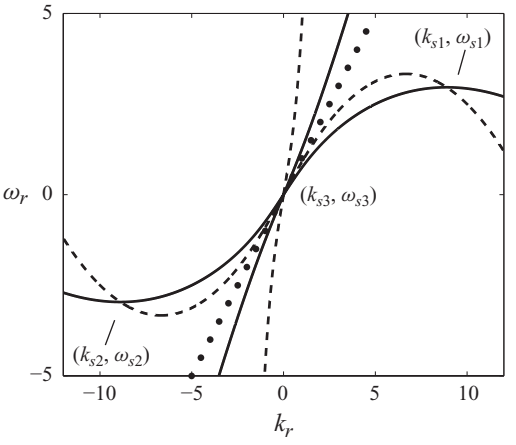

FIGURE 4. The real-valued roots of $D(k, \omega)$ (——), $\partial_k D(k, \omega)$ (— —) and $\partial_\omega D(k, \omega)$ (●) for sinuous waves with $Q = 0$ and $We = 20$. The three saddle points of (2.25) are shown.

as seen in figures 2 and 3, (5.12) may be obtained for any value of s using Hankel's formula, where $\int_C$ is $\int_{-\infty}^{0+}$ (Copson 1962).

To clarify the differences for $We > 1$, we shall remove the long-wave constraint and re-examine the analysis done by De Luca & Costa (1997) and Lin (2003) by looking at the behaviour near the saddle points of $D(k, \omega)$. The Taylor expansion about a saddle point leads to the relation $(\omega - \omega_0)^n \approx (k - k_0)^{p+2}$, allowing the Fourier integral to be simplified. Examples of this procedure can be found in both Bers (1983) and Lin (2003). Eventually, a change of variable and the use of (5.12) leads to

$$G(x, t) \approx t^{\nu-1} \exp(\mathrm{i}(k_0 x - \omega_0 t)), \tag{5.13}$$

where $\nu = n((p + 1)/(p + 2))$. This relation is especially useful when the Fourier integral cannot immediately be cast in the form of (5.12). If there are multiple saddle points, the one with the maximum growth rate is used when evaluating the response.

In the ω roots of $D(k, \omega)$ (——) given by (2.25), $\partial_k D(k, \omega)$ (— —) and $\partial_\omega D(k, \omega)$(●) are obtained for real values of k and plotted in figure 4 for $Q = 0$ and $We = 20$. For the roots of $D(k, \omega)$, this is essentially a wider view of figure 3(a). It can be seen that, for shorter waves (larger k_r), the group velocity is no longer constant and actually reverses direction. At the saddle points $(k_{s1,s2},\ \omega_{s1,s2}) \approx (\pm 9, \pm 3)$, $D(k, \omega) = \partial_k D(k, \omega) = 0$, but $\partial_\omega D(k, \omega) \neq 0$ and $\partial_{kk} D(k, \omega) \neq 0$. A Taylor expansion of $D(k, \omega)$ about this point gives to the lowest order $(k - k_{s1,s2})^2 \approx (\omega - \omega_{s1,s2})$. Recall from (2.25) that there is no exponential growth for $Q = 0$ since $\mathrm{Im}(\omega) = 0$ for all real k. By utilizing (5.13), the response to the contribution of $(k_{s1,s2},\ \omega_{s1,s2})$ becomes $G(x, t) \approx t^{-1/2}$, which is why it is stated in De Luca & Costa (1997) and Lin (2003) that these waves are actually stable for $We > 1$ and $Q = 0$. However, it can be seen that the group velocity is zero at $(k_{s1,s2},\ \omega_{s1,s2})$, and so $G(x, t) \approx t^{-1/2}$ is only valid along the ray $x/t = \mathrm{d}\omega_r/\mathrm{d}k_r = 0$. There is a finite group velocity at the saddle point $(k_{s3},\ \omega_{s3}) = (0, 0)$, where $D(k, \omega) = \partial_k D(k, \omega) = \partial_\omega D(k, \omega) = 0$, $\partial_{\omega\omega} D(k, \omega) \neq 0$ and $\partial_{kk} D(k, \omega) \neq 0$. It should be pointed out that this is also the only saddle point that arises when the long-wave approximation is used for any We. A Taylor expansion of $D(k, \omega)$ about this point gives to the lowest order $(k - k_{s3})^2 \approx (\omega - \omega_{s3})^2$. Again, utilizing (5.13), the response becomes $G(x, t) \approx t^0$ along the ray $x/t = \mathrm{d}\omega_r/\mathrm{d}k_r \neq 0$. Since decay occurs along $x/t = 0$ but not along $x/t \neq 0$, the stability should be

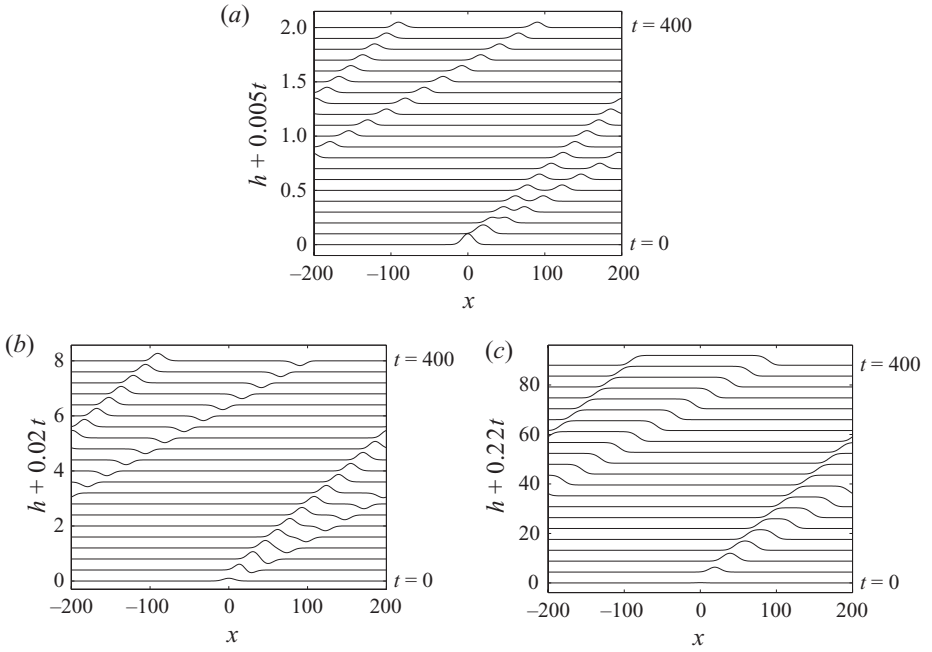

FIGURE 5. Evolution of a sinuous wave for $We = 20$, $Q = 0$. The solution (4.21) is constructed on a periodic domain of normalized length $L = 400$ using $N = 800$ modes for a duration of 400 time units. The initial disturbance velocity is given by (*a*) $[\partial_t h]_{t=0}(x) = -(\mathrm{d}h_0/\mathrm{d}x)$, (*b*) $[\partial_t h]_{t=0}(x) = 0$ and (*c*) $[\partial_t h]_{t=0}(x) = h_\delta(x)$.

considered convectively neutral by definitions (3.1) and (3.4). Previous analyses overlooked this piece of information, that only waves of zero group velocity decay. This led to the erroneous prediction of stability for $We > 1$ and $Q = 0$.

To summarize, sinuous waves in the absence of ambient gas are predicted, by both the generalized (De Luca & Costa 1997; Lin 2003) and long-wave asymptotic analysis, to be absolutely neutral for $We < 1$ and $Q = 0$. For $We > 1$, both analyses predict convective neutrality. Long sinuous waves are predicted to leave behind an origin that is exactly zero, whereas the generalized analysis predicts $t^{-1/2}$ decay at the origin. These predictions hold for any of the initial conditions listed in table 2.

Series solutions of sinuous wave evolution for $Q = 0$ are given in figure 5 for $We = 20$ and in figure 6 for $We = 0.02$. The solution (4.21) is constructed on a domain of normalized length $L = 400$ using $N = 800$ modes for both cases. The resolution is designed to accurately evolve disturbances that are longer than the sheet thickness. For $We = 20$, the Gaussian initial condition (4.23) and initial disturbance velocities (4.24) are chosen to simulate the responses $G_{sym}(x, t)$ (figure 5*a*), $G_{stat}(x, t)$ (figure 5*b*) and $G(x, t)$ (figure 5*c*) for a duration of 400 time units. For $We = 0.02$, these initial conditions are used to simulate the responses $G_{sym}(x, t)$ (figure 6*a*, ——), $G_{stat}(x, t)$ (figure 6*a*, — —) and $G(x, t)$ (figure 6*b*) for a duration of 20 time units. For $We = 20$ (figure 5), the initial disturbance expands along two downstream characteristics, as predicted in figure 3(*a*). For $We = 0.02$ (figure 6), the initial disturbance expands along upstream and downstream characteristics, as predicted in figure 3(*b*). In figures 5(*a*) and 6(*a*) (——), the split is symmetric about the point of separation. In figures 5(*b*) and 6(*a*) (— —), the split is asymmetric about the point of separation, however there is still a quiescent region between each separated wave. The impulse response, $G(x, t)$, in

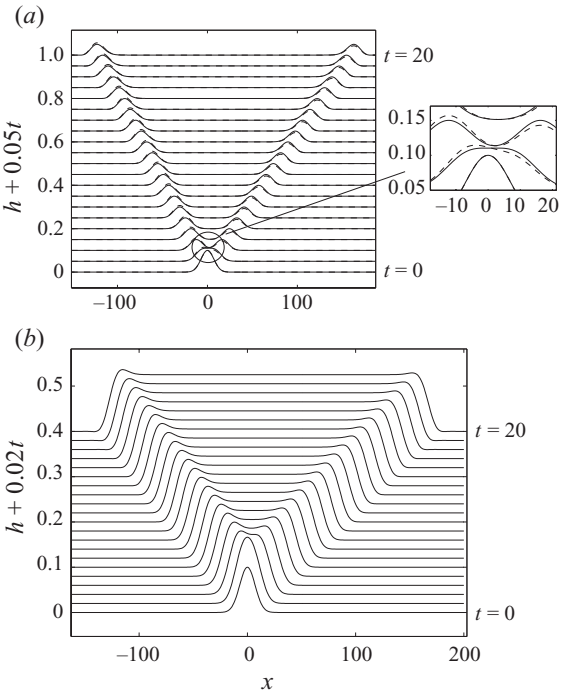

FIGURE 6. Evolution of a sinuous wave for $We = 0.02$, $Q = 0$. The solution (4.21) is constructed on a periodic domain of normalized length $L = 400$ using $N = 800$ modes for a duration of 20 time units. The initial disturbance velocity is given by (*a*) $[\partial_t h]_{t=0}(x) = -(\mathrm{d}h_0/\mathrm{d}x)$ (——), $[\partial_t h]_{t=0}(x) = 0$ (— —) and (*b*) $[\partial_t h]_{t=0}(x) = h_\delta(x)$. The inset of (*a*) indicates the asymmetry of the response when $[\partial_t h]_{t=0}(x) = 0$.

figures 5(*c*) and 6(*b*) shows no quiescent region between waves; this is reminiscent of the waveforms presented by Rosenbluth, White & Liu (1973) and Nicholson (1975) for impulsive forcing. The waves neither grow nor decay for all three responses, as indicated in figure 7(*a*) for $We = 20$ and in figure 7(*b*) for $We = 0.02$, where the maximum amplitudes (●, ▲, ■) of each response are plotted against time. This is in agreement with the neutrally stable prediction of classical theory. The origin amplitudes of $G(x, t)$(○), $G_{stat}(x, t)$(△) and G_{sym}(□) all decay for $We = 20$ (figure 7*a*), which agrees with the asymptotic prediction of convective neutrality for $We > 1$. For $We = 0.02$ (figure 7*b*), the origin neither grows nor decays, agreeing with the absolutely neutral prediction of asymptotic analysis for $We < 1$. As seen in both plots of figure 7, the origin amplitude of the responses $G_{stat}(x, t)$ and G_{sym} decays for all Weber numbers, which also agrees with the asymptotic analysis. For $We > 1$, the particular $t^{-1/2}$ decay at the origin predicted by the generalized analysis was not detected. This is a consequence of approximating the impulsive disturbance with a Gaussian. The wavenumbers used to construct the Gaussian are collected near the origin in figure 4, where all modes have a finite group velocity and the decaying stationary modes ($k_{s1,s2}$) are out of range. An investigation for large k showed dispersive waves that decay like $t^{-1/2}$. However, that is beyond the focus of this paper, to examine thin sheets ($k \ll 1$).

We now examine the stability of varicose waves in the absence of ambient gas. Here, the long-wave approximation does not eliminate saddle points as it does in the sinuous case, but it does simplify the analysis. First, we wish to find the response

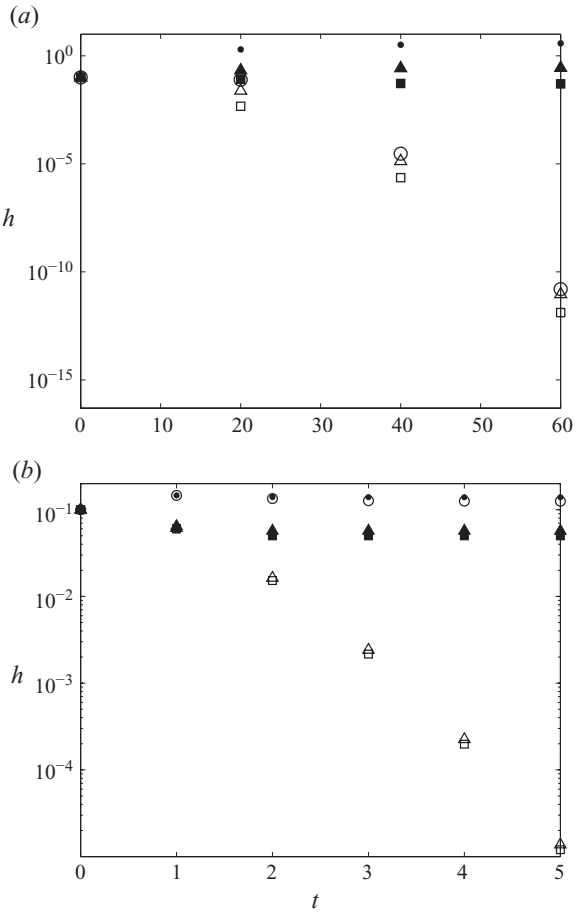

FIGURE 7. Growth of a sinuous wave for $Q=0$ and (*a*) $We=20$ (convectively neutral), (*b*) $We=0.02$ (absolutely neutral). The maximum amplitude (solid symbols) and origin amplitude (open symbols) in the series solution are compared for different initial disturbance velocities: $[\partial_t h]_{t=0}(x)=-(\mathrm{d}h_0/\mathrm{d}x)$ (■, □), $[\partial_t h]_{t=0}(x)=0$ (▲, △) and $[\partial_t h]_{t=0}(x)=h_\delta(x)$ (●, ○).

along the ray $x/t=0$. To do this, we identify the wavenumber associated with zero group velocity. The dispersive group velocity, $\mathrm{d}\omega_r/\mathrm{d}k_r=1\pm 2We^{-1/2}k$, is zero for modes of wavenumber $k_{s1,s2}=\pm We^{1/2}/2$, which corresponds with $\omega_{s1,s2}=\pm We^{1/2}/4$ for $D(k,\omega)=0$ in (5.2). A Taylor expansion of $D(k,\omega)$ about this point gives to the lowest order $(k-k_{s1,s2})^2\approx(\omega-\omega_{s1,s2})$. Then if we substitute $\omega=\omega_{s1,s2}+C_1(k-k_{1,2})^2$ into (5.4) and evaluate along the ray $x/t=0$, the response becomes

$$[h_\pm(t)]_{x/t=0}=C_2\int_{-\infty}^{\infty} f(k)\exp(-\mathrm{i}[\omega_{s1,s2}+C_1(k-k_{s1,s2})^2]t)\,\mathrm{d}k, \tag{5.14}$$

where C_1 and C_2 are functions of We only and $f(k)$ contains no singularities. By applying a change in variable and utilizing relation (5.12) we obtain

$$G_{stat}(x,t)\approx G(x,t)\approx G_{sym}(x,t)\approx t^{-1/2} \text{ along the ray } \frac{x}{t}=0. \tag{5.15}$$

To find the response along any ray $x/t=[(\mathrm{d}\omega_r/\mathrm{d}k_r)(k)]_{k_d}\neq 0$ ($k_d\neq k_{1,2}$), the group velocity of a single mode, $[(\mathrm{d}\omega_r/\mathrm{d}k_r)(k)]_{k_d}=1\pm 2We^{-1/2}k_d$, is directly substituted into

the phase of a single mode to obtain $\psi(k_d) = \pm \mathrm{i} We^{-1/2} k_d^2$. The integral (5.4) is then evaluated for all non-stationary modes, k_d:

$$[h_{\pm}(t)]_{x/t\neq 0} = C_1 \int_{-\infty}^{\infty} \hat{h}(k_d, 0) \mathrm{e}^{C_3 k_d^2 t}\, \mathrm{d}k_d + C_2 \int_{-\infty}^{\infty} \frac{\hat{h}(k_d, 0)}{k_d} \mathrm{e}^{C_3 k_d^2 t}\, \mathrm{d}k_d - \mathrm{i}C_2 \int_{-\infty}^{\infty} \frac{\partial_t \hat{h}(k_d, 0)}{k_d^2} \mathrm{e}^{C_3 k_d^2 t}\, \mathrm{d}k_d, \quad (5.16)$$

where C_1, C_2 and C_3 are functions of We only. The integrals above are set apart by the order of their k_d poles. By relation (5.12), higher order poles lead to higher order algebraic growth. If the initial disturbance velocity is impulsively perturbed ($\partial_t \hat{h}(k_d, 0) = 1$), the second order pole in the third term of (5.16) dominates the asymptotic behaviour. However, if the initial disturbance velocity is zero, the third term vanishes and the response is dominated by the first order pole in the second term of (5.16), effectively diminishing the response growth. Finally, if the initial disturbance velocity is given by $[\partial_t h]_{t=0}(x) = -\mathrm{d}h_0/\mathrm{d}x$ ($\partial_t \hat{h}(k_d, 0) = -\mathrm{i}k$), the second and third terms cancel and the response is dominated by the first term of (5.16), which contains no poles. If we subject (5.16) to the initial conditions in table 2 and make use of relation (5.12), the leading behaviour of the responses becomes

$$\left.\begin{aligned} &G_{stat}(x, t) \approx t^0 \text{ along all rays } \frac{x}{t} \neq 0, \\ &G(x, t) \approx t^{1/2} \text{ along all rays } \frac{x}{t} \neq 0, \\ &G_{sym}(x, t) \approx t^{-1/2} \text{ along all rays } \frac{x}{t} \neq 0. \end{aligned}\right\} \quad (5.17)$$

Here, the initial conditions greatly affect the response. By applying definitions (3.2)–(3.5) to (5.15) and (5.17), we find that $G_{stat}(x, t)$ is convectively neutral, $G(x, t)$ is convectively unstable and $G_{sym}(x, t)$ is stable. We can also examine the behaviour of varicose waves using Briggs' criterion (Briggs 1964). Spatial amplification curves (k_i versus k_r) of (5.2) with $Q = 0$ are shown in figure 8 for (*a*) $We = 20$ and (*b*) $We = 0.02$. All ω_i isocontours correspond to downstream propagating branches since $\mathrm{d}\omega_r/\mathrm{d}k_r > 0$ for the range of k_r shown; this can be verified in figure 3(*c*,*d*) for $\omega_i = 0$. In figure 8, the $\omega_i > 0$ isocontours are lowered until they cross $k_i = 0$; this indicates the possibility of downstream propagating convectively unstable waves. Since the cross is made at $\omega_i = 0$, exponential growth can be ruled out. Therefore, the convective instability is only possible if there is algebraic growth, which we have confirmed as $t^{1/2}$. To summarize, long varicose waves in the absence of ambient gas are convectively unstable for any Weber number. This only holds for the response, $G(x, t)$, which is initiated by impulsively disturbing both the position and velocity.

Series solutions of varicose wave evolution for $Q = 0$ and $We = 0.02$ are given in figure 9. The solution (4.21) is constructed on a domain of normalized length $L = 2 \times 10^4$ using $N = 4000$ modes. The Gaussian initial condition (4.23) and initial disturbance velocities (4.24) are chosen to simulate the responses $G_{sym}(x, t)$ (figure 9*a*), $G_{stat}(x, t)$ (figure 9*b*) and $G(x, t)$ (figure 9*c*) for a duration of 2000 time units. The initial disturbance travels downstream, as predicted in figure 3(*d*). For all responses, the origin amplitude decays, as predicted by (5.15). In figure 9(*a*), the disturbance decays as predicted by $G_{sym}(x, t) \approx t^{-1/2}$ in (5.17). This is confirmed in figure 10, where the maximum (■) and origin (□) amplitudes in the series solution fall along prediction curves $At^{-0.5}$. The amplitude, A, is specific to each curve. Both the amplitudes

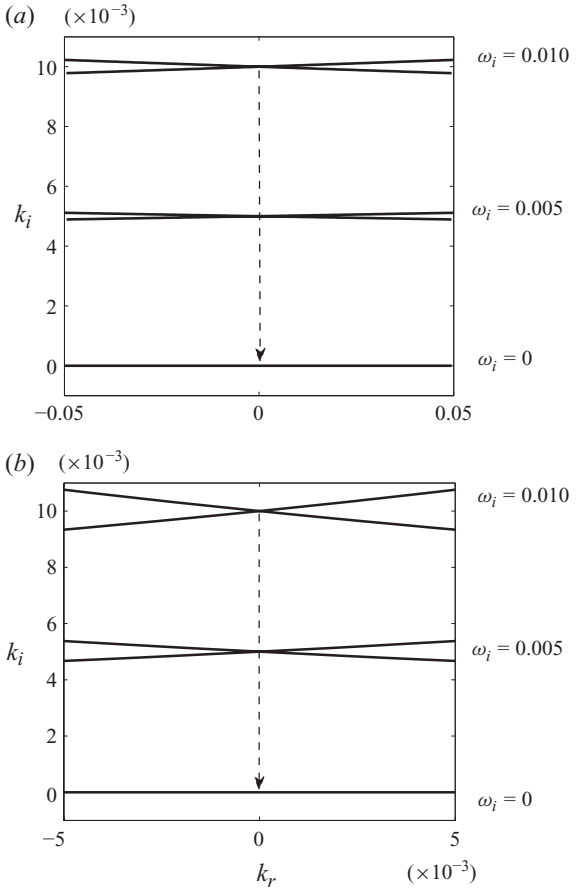

FIGURE 8. Spatial amplification plots of (5.2) for varicose waves with $Q=0$ and (*a*) $We=20$, (*b*) $We=0.02$. The branches are reduced from $\omega_i>0$ to $\omega_i=0$. The crossing of $k_i=0$ at $\omega_i=0$ indicates the possibility of algebraically convectively unstable waves.

and growth rates are found using a best fit which minimizes $||\Delta||_\infty$, where Δ is the difference between the prediction curves and the actual growth obtained from the series solution. In figure 9(*b*), the origin amplitude decays, but the maximum amplitude of the disturbance remains constant, as predicted by $G_{stat}(x,t)$ in (5.17). This is confirmed in figure 10, where the maximum amplitude (▲) appears to level off, and the origin amplitude (△) follows a prediction curve $At^{-0.5}$. In figure 9(*c*), the maximum amplitude of the disturbance grows, as predicted by $G(x,t)\approx t^{1/2}$ in (5.17). This rate is confirmed in figure 10, where the maximum amplitude in the series solution (●) falls along a prediction curve $At^{0.5}$ and the origin amplitude (○) falls along a curve $At^{-0.5}$.

The series simulation of $G_{stat}(x,t)$ is in agreement with the convectively neutral prediction of asymptotic theory, presented here for long varicose waves in the absence of ambient gas. The decay inferred by De Luca & Costa (1997) and Lin (2003), as a general prediction, was only detected at the origin. The series simulation of $G(x,t)$ is in agreement with the convectively unstable prediction of asymptotic theory, presented here for long varicose waves in the absence of ambient gas. This is a new type of

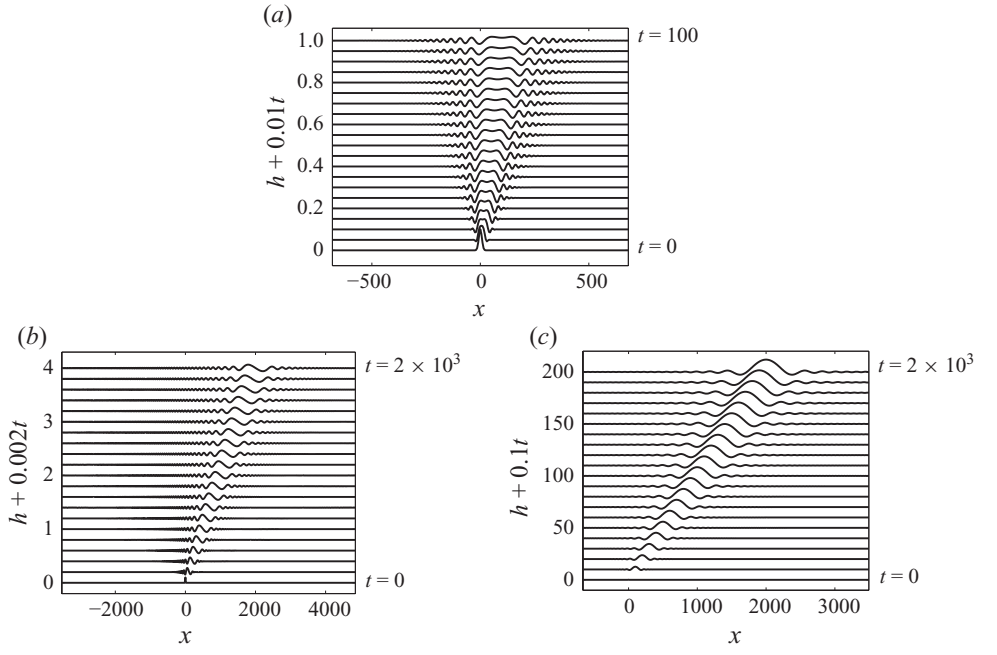

FIGURE 9. Evolution of a varicose wave for $We = 0.02$, $Q = 0$. The solution (4.21) is constructed on a periodic domain of normalized length $L = 2 \times 10^4$ using $N = 4000$ modes for a duration of 2000 time units. The initial disturbance velocity is given by (*a*) $[\partial_t h]_{t=0}(x) = -(\mathrm{d}h_0/\mathrm{d}x)$, (*b*) $[\partial_t h]_{t=0}(x) = 0$ and (*c*) $[\partial_t h]_{t=0}(x) = h_\delta(x)$. For clarity, the evolution has been truncated to 100 time units in (*a*).

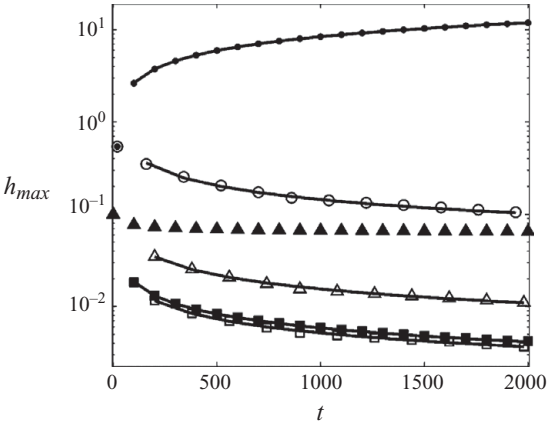

FIGURE 10. Growth of a varicose wave for $Q = 0$ and $We = 0.02$. The maximum amplitude (solid symbols) and origin amplitude (open symbols) in the series solution are compared for different initial disturbance velocities: $[\partial_t h]_{t=0}(x) = -(\mathrm{d}h_0/\mathrm{d}x)$ (■, □), $[\partial_t h]_{t=0}(x) = 0$ (▲, △) and $[\partial_t h]_{t=0}(x) = h_\delta(x)$ (●, ○). The spatio-temporal prediction curves (——) are given (from bottom to top) by $At^{-0.5}$, $At^{-0.5}$, $At^{-0.5}$, $At^{-0.5}$ and $At^{0.5}$. The amplitude A is specific to each curve.

algebraic instability for convective growth, similar to the algebraic instability for absolute growth discovered by De Luca & Costa (1997) and examined later in § 5.2. While this is in disagreement with all previous predictions, it should be mentioned that, although Squire (1953), De Luca & Costa (1997) and Lin (2003) indicate that

varicose waves do not become unstable for $Q=0$, the actual analysis is always left for the reader, since the focus has been the 'dominant' sinuous mode. We have shown here that, in the absence of ambient gas, the varicose mode is actually the dominant mode for instability. The series simulation of $G_{sym}(x,t)$ is stable, which is also in agreement with the asymptotic predictions. This response illustrates that certain initial conditions can affect the growth rate by reducing the order of singularities in the Fourier integral. For the remaining results, only $G_{stat}(x,t)$ and $G(x,t)$ are examined, as $G_{sym}(x,t)$ provides no additional insight within the scope of this work.

5.2. *Presence of ambient gas ($Q \neq 0$)*

With the inclusion of ambient gas, direct computation of the Fourier integrals becomes exhaustive, and the long-wave approximation does little to reduce the complexity. We instead, examine the behaviour near the saddle points of (2.25) and (2.32). For sinuous or varicose waves, the $\pm$ branches of the Fourier integrals (2.26) and (2.33) can be written like

$$h_{\pm}(x,t) = \int_{-\infty}^{\infty} \left[f_1(k)\ \hat{h}(k,0) + \frac{f_2(k)\partial_t \hat{h}(k,0)}{(\partial D/\partial\omega)_{\omega_{\pm}(k)}} \right] \mathrm{e}^{\psi(k)t}\,\mathrm{d}k, \tag{5.18}$$

where $f_1(k)$ contains no non-removable singularities, $f_2(k)$ contains no singularities and is non-zero at $k=0$ and $\psi(k)=\mathrm{i}[k(x/t)-\omega_{\pm}(k)]$.

The real components of the ω roots of $D(k,\omega)$ (——), $\partial_k D(k,\omega)$ (– –) and $\partial_\omega D(k,\omega)$ (●) are obtained for real values of k and plotted in figure 11 for sinuous waves and in figure 12 for varicose waves with $We=20$ and $Q=0.0013$ (water–air). The imaginary component of ω is given in figure 2. The behaviour appears similar to the $Q=0$ behaviour in figure 4, as they share the $(k_{s1,s2},\omega_{s1,s2}) \approx (\pm 9, \pm 3)$ saddle point. However, the magnification in figure 11(*b*) shows that an additional saddle point pair is found at $(k_{s3,s4},\omega_{s3,s4}) \approx (\pm 0.025, \pm 0.023 + \pm \mathrm{i}0.0025)$. For all four saddle points, $D(k,\omega)=\partial_k D(k,\omega)=0$ but $\partial_\omega D(k,\omega)\neq 0$ and $\partial_{kk} D(k,\omega)\neq 0$. A Taylor expansion of $D(k,\omega)$ about these points gives to the lowest order $(k-k_{s1-s4})^2 \approx (\omega-\omega_{s1-s4})$, which reduces (5.18) to

$$h_j(x,t) = \int_{-\infty}^{\infty} f(k)\exp(\mathrm{i}[k(x/t)-\omega_j - C(k-k_{sj})^2]t)\,\mathrm{d}k \quad (j=1,2,3,4), \tag{5.19}$$

where $f(k)$ contains no singularities and C is a function of We and Q only. The points $(k_{s1,s2},\omega_{s1,s2})$ are valid along the ray $x/t=\mathrm{d}\omega_r/\mathrm{d}k_r=0$. Since $\omega_{s1,s2}$ is real, there is no exponential growth. By utilizing (5.12) and applying a change of variable to (5.19), the behaviour of the responses becomes

$$G(x,t) \approx G_{stat}(x,t) \approx t^{-1/2} \text{ along the ray } \frac{x}{t} = \frac{\mathrm{d}\omega_r}{\mathrm{d}k_r} = 0. \tag{5.20}$$

The points $(k_{s3,s4},\omega_{s3,s4})$ are valid along the ray $x/t=\mathrm{d}\omega_r/\mathrm{d}k_r\neq 0$. By utilizing (5.12) and a change of variable, the behaviour of the responses becomes

$$G(x,t) \approx G_{stat}(x,t) \approx t^{-1/2}\exp(\max\,[\mathrm{Im}(\omega_{s3})]\,t) \text{ along the ray } x/t = \mathrm{d}\omega_r/\mathrm{d}k_r \neq 0, \tag{5.21}$$

where $\max[\mathrm{Im}(\omega_{s3})]>0$. The above responses describe a convectively unstable disturbance, given by definitions (3.3) and (3.4). This not only applies to sinuous and varicose waves for $We>1$ and $Q\neq 0$, but also to varicose waves with $We<1$ and $Q\neq 0$. The exponential growth rate, $\max[\mathrm{Im}(\omega_{s3})]$, can be obtained from figure 2

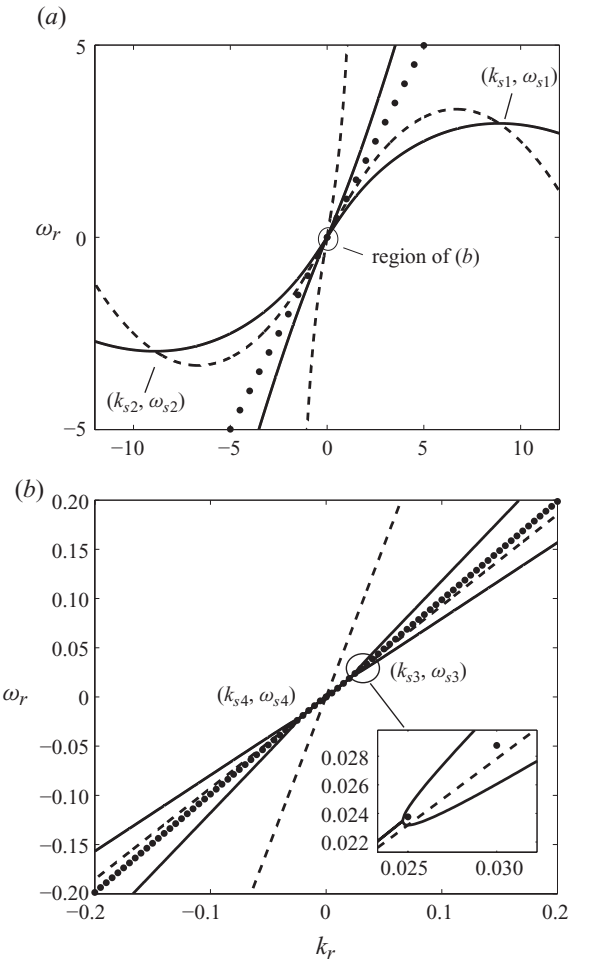

FIGURE 11. The real component of the ω roots of $D(k, \omega)$ (——), $\partial_k D(k, \omega)$ (− −) and $\partial_\omega D(k, \omega)$ (●) plotted against real k values for sinuous waves with $Q = 0.0013$ and $We = 20$. The four saddle points of (2.25) are shown. The imaginary component of ω is given in figure 2(*a*).

for each case. These stability predictions have been previously stated by De Luca & Costa (1997) and Lin (2003).

The series solutions in figures 13–15 are constructed using $N = 4000$ modes and given the Gaussian initial condition (4.23) and initial disturbance velocity $[\partial_t h]_{t=0}(x) = 0$ in order to simulate the response $G_{stat}(x, t)$. A simulation of the response $G(x, t)$, which is associated with the initial disturbance velocity $[\partial_t h]_{t=0}(x) = h_\delta(x)$, is not shown here because, for the following cases, the behaviour is qualitatively the same. Nevertheless, the actual growth is recorded in figure 16 for both initial disturbance velocities, $[\partial_t h]_{t=0}(x) = 0$ (▲) and $[\partial_t h]_{t=0}(x) = h_\delta(x)$ (●).

A series solution of sinuous wave evolution for $We = 20$ and $Q = 0.0013$ is shown in figure 13. The solution is constructed on a domain of normalized length $L = 5000$ and evolved for a duration of 10^4 time units. The disturbance travels downstream, as predicted in figure 3(*a*), and convectively grows like $t^{-1/2}e^{0.0025t}$, as predicted by (5.21) and figure 2(*a*). This rate is confirmed in figure 16(*a*), where the maximum amplitude

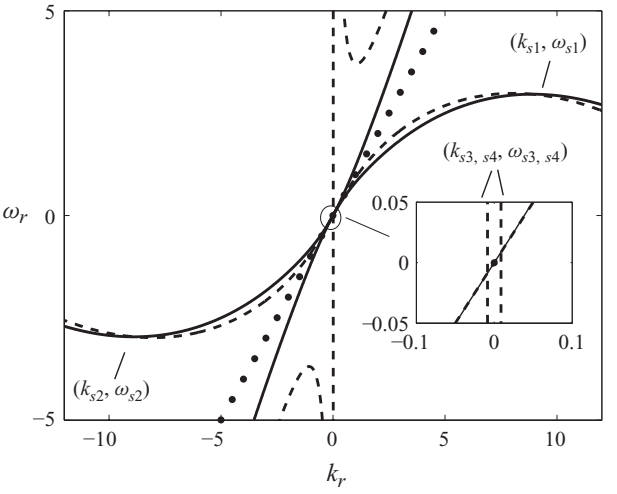

FIGURE 12. The real component of the ω roots of $D(k, \omega)$ (——), $\partial_k D(k, \omega)$ (– –) and $\partial_\omega D(k, \omega)$ (●) plotted against real k values for varicose waves with $Q = 0.0013$ and $We = 20$. The four saddle points of (2.25) are shown. The inset shows the nearly vertical 'line' of $\partial_k D(k, \omega)$ as actually *two* lines, which form saddle points $(k_{s3,s4}, \omega_{s3,s4})$. The imaginary component of ω is given in figure 2(*b*).

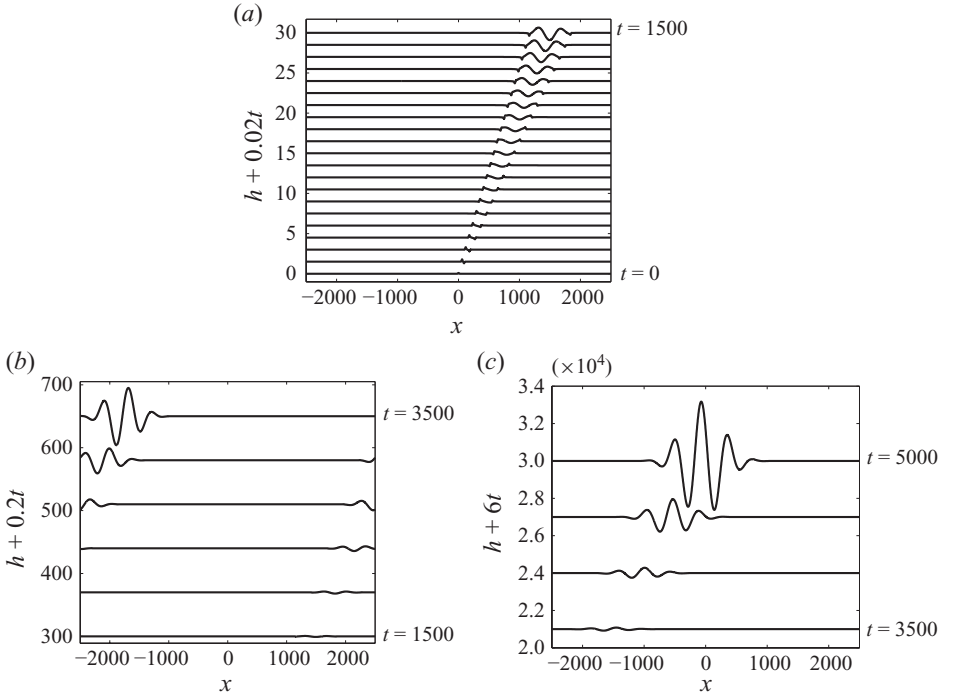

FIGURE 13. Evolution of a sinuous wave for $We = 20$, $Q = 0.0013$. The solution (4.21) is constructed on a periodic domain of normalized length $L = 5000$ using $N = 4000$ modes for a duration of 10^4 time units. The initial disturbance velocity is given by $[\partial_t h]_{t=0}(x) = 0$. For clarity, the evolution has been truncated to 5000 time units.

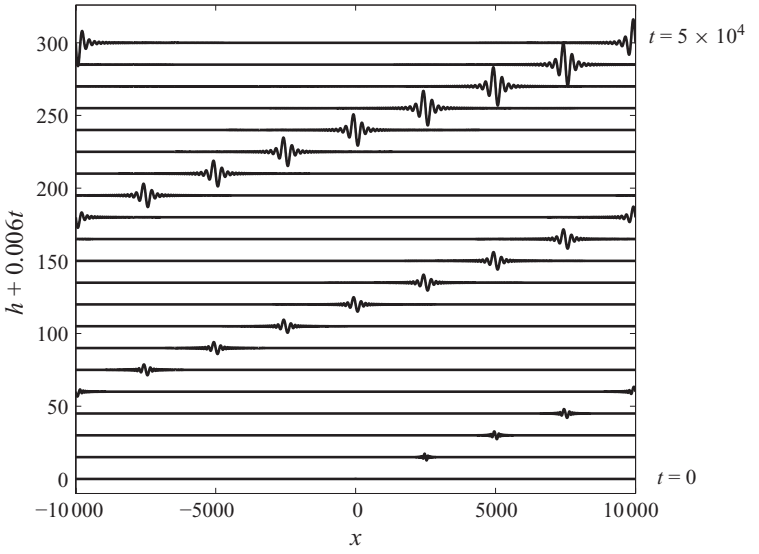

FIGURE 14. Evolution of a varicose wave for $We = 20$, $Q = 0.0013$. The solution (4.21) is constructed on a periodic domain of normalized length $L = 2 \times 10^4$ using $N = 4000$ modes for a duration of 2×10^5 time units. The initial disturbance velocity is given by $[\partial_t h]_{t=0}(x) = 0$. For clarity, evolution has been truncated to 5×10^4 time units.

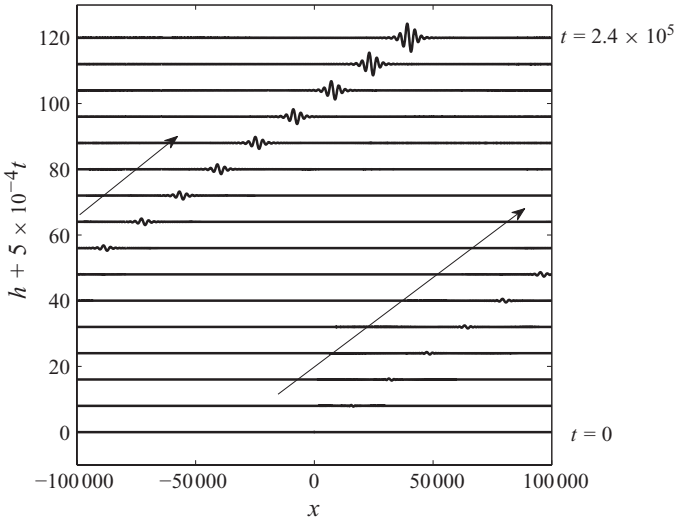

FIGURE 15. Evolution of a varicose wave for $We = 0.02$, $Q = 0.13$. The solution (4.21) is constructed on a periodic domain of normalized length $L = 2 \times 10^5$ using $N = 4000$ modes for a duration of 1.2×10^6 time units. The initial disturbance velocity is given by $[\partial_t h]_{t=0}(x) = 0$. For clarity, evolution has been truncated to 2.4×10^5 time units.

in the series solution is compared with the classical (— —) and asymptotic (——) prediction curves, $Ae^{0.0025t}$ and $At^{0.5}e^{0.0025t}$.

A series solution of varicose wave evolution for $We = 20$ and $Q = 0.0013$ is shown in figure 14. The solution is constructed on a domain of normalized length $L = 2 \times 10^4$ and evolved for a duration of 2×10^5 time units. The disturbance travels downstream, as predicted in figure 3(*c*), and convectively grows like $t^{-1/2}e^{4.9 \times 10^{-5}t}$, as predicted

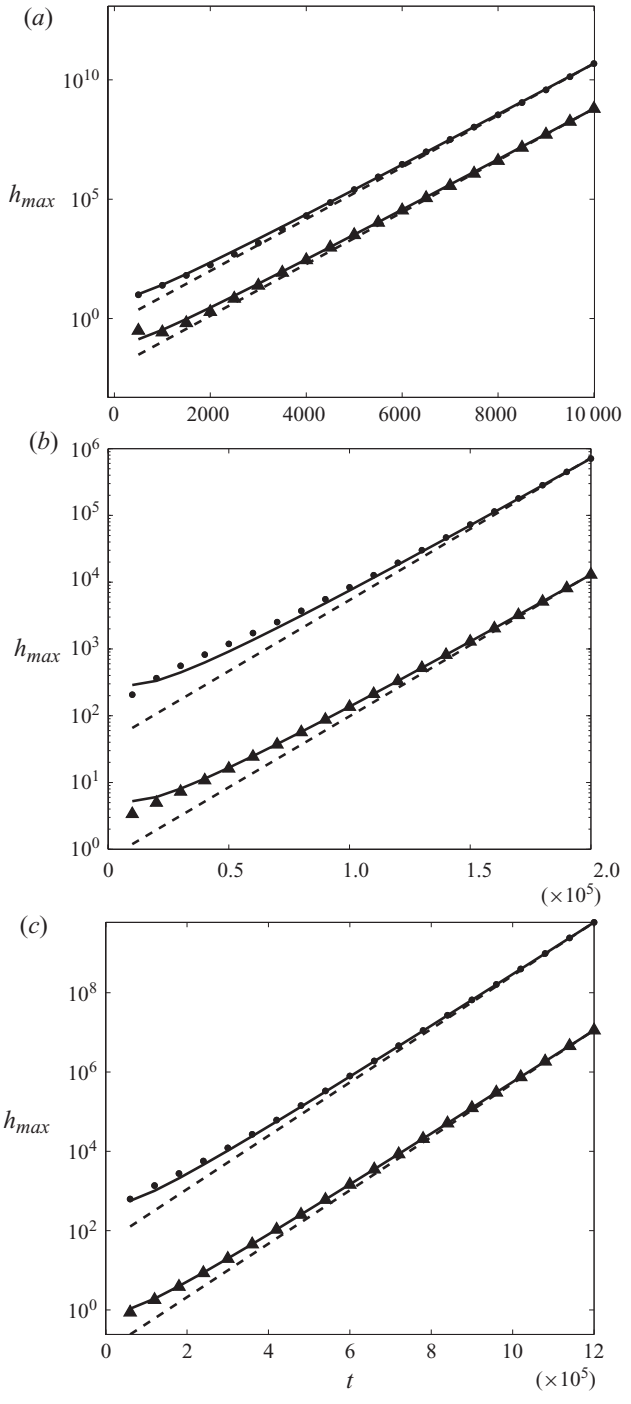

FIGURE 16. The maximum amplitude in the series solution is compared for initial disturbance velocities, $[\partial_t h]_{t=0}(x) = 0$ (▲) and $[\partial_t h]_{t=0}(x) = h_\delta(x)$ (●). (*a*) Sinuous, $We = 20$, $Q = 0.0013$, $\max(\omega_i) = 0.0025$ (cf. figure 2*a*) ; (*b*) varicose, $We = 20$, $Q = 0.0013$, $\max(\omega_i) = 4.9 \times 10^{-5}$ (cf. figure 2*b*); (*c*) varicose, $We = 0.02$, $Q = 0.13$, $\max(\omega_i) = 1.55 \times 10^{-5}$ (cf. figure 2*c*). Classical (– –) and asymptotic (——) prediction curves in each plot are given (from bottom to top) by $Ae^{\max(\omega_i)t}$, $At^{0.5}e^{\max(\omega_i)t}$, $Ae^{\max(\omega_i)t}$ and $At^{0.5}e^{\max(\omega_i)t}$. The amplitude, A, is specific to each curve.

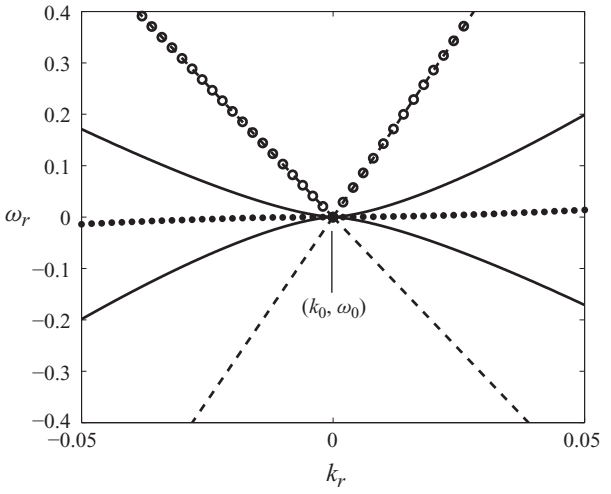

FIGURE 17. The real component of the ω roots of $D(k,\omega)$ (——), $\partial_k D(k,\omega)$ (− −), $\partial_\omega D(k,\omega)$ (●) and $\partial_{kk} D(k,\omega)$ (○) for sinuous waves with $Q = 0.13$ and $We = 0.02$. The imaginary component of ω is zero, as indicated figure 2(*a*).

by (5.21) and figure 2(*b*). This rate is confirmed in figure 16(*b*), where the maximum amplitude in the series solution is compared with the classical (− −) and asymptotic (——) prediction curves, $A\exp(4.9\times10^{-5}t)$ and $At^{0.5}\exp(4.9\times10^{-5}t)$.

A series solution of varicose wave evolution for $We = 0.02$ and $Q = 0.13$ is shown in figure 15. The solution is constructed on a domain of normalized length $L = 2\times10^5$ and evolved for a duration of 1.2×10^6 time units. The disturbance travels downstream, as predicted in figure 3(*d*), and convectively grows like $t^{-1/2}\exp(1.55\times10^{-5}t)$, as predicted by (5.21) and figure 2(*c*). This rate is confirmed in figure 16(*c*), where the maximum amplitude in the series solution is compared with the classical (− −) and asymptotic (——) prediction curves, $A\exp(1.55\times10^{-5}t)$ and $At^{0.5}\exp(1.55\times10^{-5}t)$.

The series solutions in figures 13–15 are all convectively unstable and grow exponentially as predicted by classical and asymptotic stability theory. As seen in figure 16, the additional $t^{-1/2}$ decay is also resolved, which lends more credit to the asymptotic theory for predicting the transient behaviour. While the growth rates remain identical for either initial disturbance velocity, the initial condition $[\partial_t h]_{t=0}(x) = h_\delta(x)$ causes a larger disturbance amplitude, which can be seen when comparing the upper and lower curves in figure 16.

We shall now examine the stability of sinuous waves in the presence of ambient gas with $We < 1$. The real components of the ω roots of $D(k,\omega)$ (—), $\partial_k D(k,\omega)$ (− −), $\partial_\omega D(k,\omega)$(●) and $\partial_{kk} D(k,\omega)$(○) are obtained for real k values and plotted in figure 17 for $We = 0.02$ and $Q = 0.13$. The imaginary component of ω is zero, as shown in figure 2(*a*). There is an apparent saddle point at $(k_0,\omega_0) = (0,0)$, where $D(k,\omega) = \partial_k D(k,\omega) = \partial_{kk} D(k,\omega) = \partial_\omega D(k,\omega) = 0$ but $\partial_{\omega\omega} D(k,\omega) \neq 0$ and $\partial_{kkk} D(k,\omega) \neq 0$. It should be noted, however, that the dispersion relation (2.25) is non-smooth at $k_r = 0$ because of the $\mathrm{sgn}(k_r)$ term. It is more accurate to say that the saddle point exists at $(k_0,\omega_0) = (0^\pm, 0^\pm)$, which is valid along the ray $x/t = \mathrm{d}\omega_r/\mathrm{d}k_r = 0$. Since ω_0 is real, there is no exponential growth. A Taylor expansion of $D(k,\omega)$ about this point gives, to the lowest order, $(k-k_0)^3 \approx (\omega-\omega_0)^2$, which

reduces (5.18) to

$$[h_{\pm}(x,t)]_{x/t=0} = \int_{-\infty}^{\infty} \left[f_1(k)\ \hat{h}(k,0) + \frac{f_2(k)\partial_t \hat{h}(k,0)}{2k^{3/2}} \right] \mathrm{e}^{-\mathrm{i}k^{3/2}t}\,\mathrm{d}k, \tag{5.22}$$

where $f_1(k) = \mathrm{sgn}(k_r)Q + k - 2k^{1/2}$ and $f_2(k) = \mathrm{i}[\mathrm{sgn}(k_r)Q + k]$. The even symmetry of the integrand allows us to replace $\int_{-\infty}^{\infty}$ with $2\int_0^{\infty}$ so that (5.22) may be evaluated using Hankel's formula (Copson 1962). This effectively bypasses the non-analytic point $k_r = 0$. If the initial disturbance velocity is zero ($\partial_t \hat{h}(k,0) = 0$), the second term in (5.22) vanishes, leading to a Green's function with no singularities. This is the assumption made in Luchini (2004, equation (3)). However, if the initial disturbance velocity is impulsively perturbed ($\partial_t \hat{h}(k,0) = 1$), the second term remains and the $k^{3/2}$ singularity leads to growth. If we subject (5.22) to the initial conditions in table 2 and make use of relation (5.12), the leading behaviour of the responses along the ray $x/t = 0$ becomes

$$\left.\begin{aligned} G_{stat}(x,t) \approx t^{-2/3} \text{ along the ray } \frac{x}{t} = \frac{\mathrm{d}\omega_r}{\mathrm{d}k_r} = 0, \\ G(x,t) \approx t^{1/3} \text{ along the ray } \frac{x}{t} = \frac{\mathrm{d}\omega_r}{\mathrm{d}k_r} = 0. \end{aligned}\right\} \tag{5.23}$$

It can be shown by applying the method of stationary phase to (5.18) and remembering that $\omega_i = 0$ for all real k (figure 2*a*) that

$$G_{stat}(x,t) \approx t^{-1/2} \text{ along the ray } \frac{x}{t} = \frac{\mathrm{d}\omega_r}{\mathrm{d}k_r} \neq 0. \tag{5.24}$$

The response, $G(x,t)$, describes an absolutely unstable wave, as defined by (3.5), which is the result previously obtained by De Luca & Costa (1997) and derived in (Lin 2003). The static response, $G_{stat}(x,t)$, describes a stable wave, which is the result obtained by Luchini (2004). We can also examine the behaviour using Briggs' criterion (Briggs 1964). A spatial amplification curve of (2.25) with $Q = 0.13$ and $We = 0.02$ is shown in figure 18. The downstream (——) and upstream (— —) branches associated with each ω_i isocontour are reduced from $\omega_i > 0$ to the 'pinch' point, where the branches coalesce ($\mathrm{d}\omega_r/\mathrm{d}k_r = 0$). A temporally growing wave with zero group velocity describes an absolutely unstable wave, as defined by (3.5). Since $\omega_i = 0$ at the pinch point, the absolute instability is only possible if there is algebraic growth, which we have confirmed as $t^{1/3}$.

It should be noted that Luchini (2004) remarks on the existence of a zero-wavenumber time-growing solution for the d'Alembert wave equation, when the velocity is impulsively perturbed. As he states, this is a non-physical solution. In contrast to the wave equation, however, the integral solution for a planar liquid sheet with $We < 1$ and $Q \neq 0$ has convergent behaviour near the origin of wavenumber space, as shown in figure 17. Furthermore, it is the accumulation of modes which leads to $t^{1/3}$ growth, and not the contribution of any single mode. In fact, the results given below were obtained by excluding the $k = 0$ mode, because it is undefined in the $\mathrm{sgn}(k_r)$ function.

Series solutions of sinuous wave evolution for $We = 0.02$ and $Q = 0.13$ are constructed using $N = 4000$ modes on a domain of normalized length $L = 2 \times 10^4$ and are shown in figure 19 for a magnified region. The Gaussian initial condition (4.23) and initial disturbance velocities $[\partial_t h]_{t=0}(x) = 0$ and $[\partial_t h]_{t=0}(x) = h_\delta(x)$ are chosen to simulate the responses $G_{stat}(x,t)$ (figure 19*a*) and $G(x,t)$ (figure 19*b*) for a duration

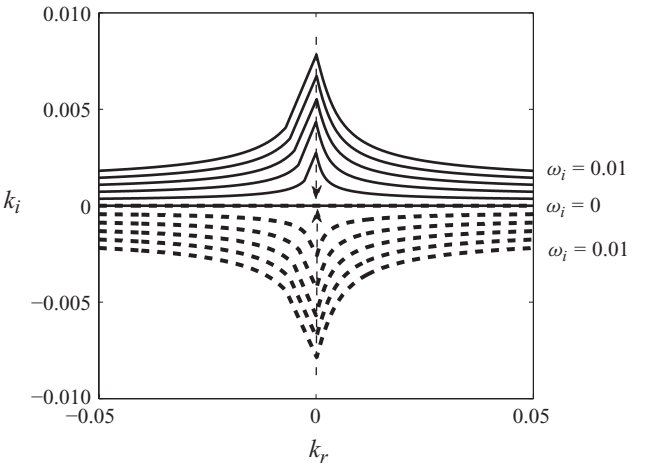

FIGURE 18. Spatial amplification plot of (2.25) for sinuous waves with $Q = 0.13$ and $We = 0.02$. The downstream (——) and upstream (— —) branches are reduced from $\omega_i > 0$ to $\omega_i = 0$. The branches meet at a pinch point where $\omega_i = 0$, indicating the possibility of algebraically absolutely unstable waves.

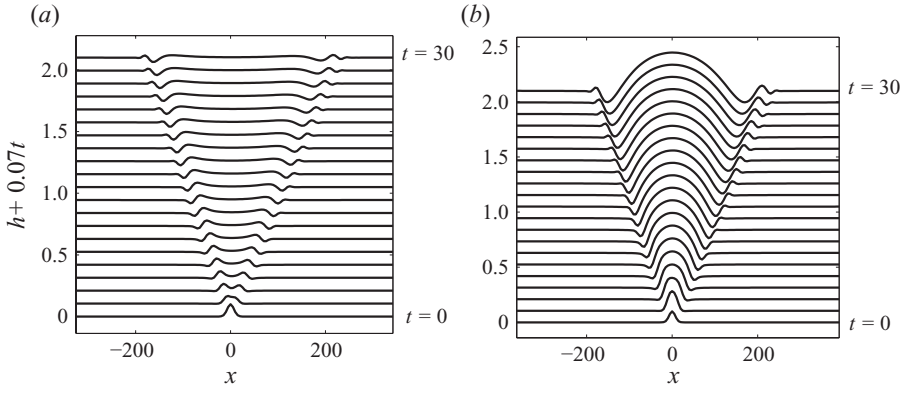

FIGURE 19. Evolution of a sinuous wave for $We = 0.02$, $Q = 0.13$. The solution (4.21) is constructed on a periodic domain of normalized length $L = 2 \times 10^4$ using $N = 4000$ modes for a duration of 1200 time units. The initial disturbance velocity is given by (*a*) $[\partial_t h]_{t=0}(x) = 0$ and (*b*) $[\partial_t h]_{t=0}(x) = h_\delta(x)$. For clarity, the evolution for both responses has been truncated to 30 time units and the domain has been magnified.

of 1200 time units. For either case, the disturbance spreads both upstream and downstream, as predicted in figure 3(*b*). For the case where the initial disturbance velocity is $[\partial_t h]_{t=0}(x) = 0$, the maximum (▲) and origin (△) amplitudes are plotted against time in figure 20. The maximum amplitude falls along the curve $At^{-0.5}$, as predicted by (5.24). The origin amplitude falls along the curve $At^{-0.6667}$, as predicted by $G_{stat}(x, t)$ in (5.23). For the case where the initial disturbance velocity is $[\partial_t h]_{t=0}(x) = h_\delta(x)$, the maximum (●) and origin (○) amplitudes are also plotted against time in figure 20. The origin amplitude falls along the curve $At^{0.3333}$ as predicted by $G(x, t)$ in (5.23). Here, the maximum amplitude is the origin amplitude.

For the case of $We < 1$ and $Q \neq 0$, the series solutions do not agree with the neutral stability prediction of classical stability theory. The response $G_{stat}(x, t)$ agrees with the stable (decaying) prediction of Luchini (2004), while the response $G(x, t)$ agrees

Wave	Q	We	Growth along $x/t=0$	Growth along $x/t=$ constant	Spatio-temporal behaviour
Sinuous	$=0$	>1	0	t^0	Convectively neutral
Sinuous	$=0$	<1	t^0, 0	t^0	Neutral (absolutely, convectively)
Sinuous	$\neq 0$	>1	$t^{-1/2}$	$t^{-1/2}e^{\max(\omega_i)t}$	Convectively unstable
Sinuous	$\neq 0$	<1	$t^{1/3}$, $t^{-2/3}$	$t^{1/3}$, $t^{-1/2}$	Absolutely unstable, stable
Varicose	$=0$	Any	$t^{-1/2}$	$t^{1/2}$, $t^{-1/2}$	Convectively unstable, stable
Varicose	$\neq 0$	Any	$t^{-1/2}$	$t^{-1/2}e^{\max(\omega_i)t}$	Convectively unstable

TABLE 3. Asymptotic growth predictions for sinuous and varicose waves in a thin sheet with an initial disturbance given by either $\{h(x,0)=\partial_t h(x,0)=\delta(x)\}$ or $\{h(x,0)=\delta(x), \partial_t h(x,0)=0\}$. Two growth rates and stability types are provided where the response to these condition differ.

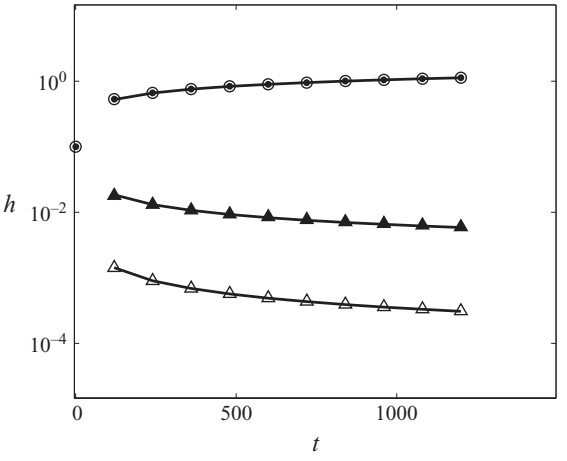

FIGURE 20. Growth of a sinuous wave for $We=0.02$, $Q=0.13$. The maximum amplitude (solid symbols) and origin amplitude (open symbols) in the series solution are shown for initial disturbance velocities, $[\partial_t h]_{t=0}(x)=0$ (▲, △) and $[\partial_t h]_{t=0}(x)=h_\delta(x)$ (●, ○). These are compared with the spatio-temporal prediction curves: $At^{-0.6667}$ (bottom), $At^{-0.5}$ (middle) and $At^{0.3333}$ (top). The amplitude, A, is specific to each curve.

with the absolutely unstable prediction of De Luca & Costa (1997). A review of the asymptotic stability predictions of this section are given in table 3.

6. Conclusions

Series solutions not only confirm the asymptotic predictions listed in table 3 for thin sheets, but also allow us to assess the general value of classical versus spatio-temporal linear stability theory and the interpretation of asymptotic predictions. Classical theory has the limitation of only being able to predict exponential growth. If the growth is in fact algebraic, the classical theory falsely interprets this as neutral stability. Another limitation of the classical theory is that it is blind to the nature of growth (convective or absolute). These points have been made as early as Sturrock (1958) and as recently as Lin & Wang (2008). Here, the series solutions provide actual validation. The long-term algebraic growth arises from the *accumulation* of Fourier modes. This contrasts with exponential growth, which can be paired with a *specific* mode on a temporal stability plot.

Spatio-temporal theory relies on the asymptotic evaluation of the Green's function, taken here as the Fourier integral solution subject to an initial impulse. Recent disagreements in the literature stem from each author's interpretation of the Green's function and whether or not it contains singularities. Here, we show that the order of singularities in the Green's function is directly related to the choice of initial conditions.

Series solutions of varicose waves confirm that, for $Q = 0$, an initial Gaussian perturbation of position leads to neutral stability, whereas a perturbation of both position and velocity leads to convective instability where the disturbance grows like $t^{1/2}$. This is true for any Weber number. It should be pointed out that this $t^{1/2}$ growth is a new result. None of the previous linear analyses predict instability for varicose waves when $Q = 0$ (Squire 1953; Hagerty & Shea 1955; De Luca & Costa 1997; Lin 2003). Since sinuous waves do not grow at all for $Q = 0$, varicose waves would appear to be the dominant mode in the absence of ambient gas.

For sinuous waves where $Q \neq 0$ and $We < 1$, series solutions confirm that an initial Gaussian perturbation of position leads to decay like $t^{-1/2}$ away from the origin and $t^{-2/3}$ at the origin, which corresponds with the prediction of Luchini (2004). If both the position and velocity are perturbed, the disturbance becomes absolutely unstable and grows in all directions like $t^{1/3}$, which is the prediction of De Luca & Costa (1997). The question then becomes: which initial conditions accurately represent a physical disturbance? Evidence suggests that this may depend on the experimental configuration.

The experiments of Brown (1961) seem to indicate absolute instability for $We < 1$ in lacquer sheets, which suggests that the initial conditions leading to growth are more relevant. Also, Crapper *et al.* (1973) observed non-exponential growth of waves in plane water sheets, which they linked to boundary layer separation. In a nonlinear stability analysis of plane sheets, Jazayeri & Li (2000) found that higher-order harmonics of the solution may be responsible for sheet breakup. Nevertheless, the transient push towards nonlinear growth and atomization could still be attributed to an algebraic absolute instability. This explanation was given by Lin & Jiang (2003) to describe the instability that leads to the rupture and termination of a radially expanding liquid sheet.

On the other hand, Roche *et al.* (2006) observed ruptures in falling sheets with $We < 1$ that subsequently heal, returning the sheet to a stable state. In the experiments of Le Grand-Piteira *et al.* (2006), falling sheets were reported to withstand relatively high amplitude sinuous oscillations without sheet rupture. Since these experiments seem to contradict linear analyses, the authors conjectured that a nonlinear approach is the only practical method of explanation. Another possible explanation, suggested by De Luca & Costa (1997) , is that viscosity may act as a stabilizing agent, suppressing the algebraic growth that leads to breakup. It is clear that more experiments are necessary, as well as an analysis including both viscous and nonlinear effects.

This work was supported in part by NSF Grant No. CTS-0138057.

REFERENCES

Barlow, N. S., Helenbrook, B. T., Lin, S. P. & Weinstein, S. J. 2010 An interpretation of absolutely and convectively unstable waves using series solutions. *Wave Motion* doi:10.1016/j.wavemoti.2010.04.003.

Bender, C. M. & Orszag, S. A. 1978 *Advanced Mathematical Methods for Scientists and Engineers I: Asymptotic Methods and Perturbation Theory*. McGraw-Hill.

Bers, A. 1983 Space–time evolution of plasma instabilities-absolute and convective. In *Handbook of Plasma Physics, vol. 1: Basic Plasma Physics 1* (ed. A. A. Galeev & R. Z. Sagdeev), chap. 3.2, pp. 451–517. North-Holland.

Bers, A. & Briggs, R. J. 1964 Criteria for determining absolute instabilities and distinguishing between amplifying and evanescent waves. *Bull. Am. Phys. Soc.* **9**, 304.

Briggs, R. J. 1964 *Electron-Stream Interaction with Plasmas*. MIT Press.

Brown, D. R. 1961 A study of the behaviour of a thin sheet of moving liquid. *J. Fluid Mech.* **10**, 297–305.

Copson, E. T. 1962 *An Introduction to the Theory of Functions of a Complex Variable*. Oxford University Press.

Crapper, G. D., Dombrowski, N., Jepson, W. P. & Pyott, G. A. D. 1973 A note on the growth of Kelvin–Helmholtz waves on thin liquid sheets. *J. Fluid Mech.* **57**, 671–672.

De Luca, L. & Costa, M. 1997 Instability of a spatially developing liquid sheet. *J. Fluid Mech.* **331**, 127–144.

Gaster, M. 1968 Growth of disturbances in both space and time. *J. Fluid Mech.* **11** (4), 723–727.

Hagerty, W. W. & Shea, J. F. 1955 A study of the stability of plane fluid sheets. *J. Appl. Mech.* **22**, 509–514.

Huerre, P. 1987 Spatio-temporal instabilities in closed and open flows. In *Instabilities and Nonequilibrium Structures* (ed. E. Tirapegui & D. Villarroel), vol. 1, pp. 141–177. D. Reidel.

Huerre, P. & Monkewitz, P. A. 1990 Local and global instabilities in spatially developing flows. *Annu. Rev. Fluid Mech.* **22**, 473–537.

Jazayeri, S. A. & Li, X. 2000 Nonlinear instability of plane liquid sheets. *J. Fluid Mech.* **406**, 281–308.

Le Grand-Piteira, N., Brunet, P., Lebon, L. & Limat, L. 2006 Propagating wave pattern on a falling liquid curtain. *Phys. Rev. Lett.* E **74** (2), 026305.

Lin, S. P. 2003 *Breakup of Liquid Sheets and Jets*. Cambridge University Press.

Lin, S. P. & Jiang, W. Y. 2003 Absolute and convective instability of a radially expanding liquid sheet. *Phys. Fluids* **15** (6), 1745–1754.

Lin, S. P., Lian, Z. W. & Creighton, B. J. 1990 Absolute and convective instability of a liquid sheet. *J. Fluid Mech.* **220**, 673–689.

Lin, S. P. & Wang, Z. L. 2008 Three types of linear theories for atomizing liquids. *Atomization Sprays* **18** (3), 273–286.

Luchini, P. 2004 Is a plane liquid curtain algebraically absolutely unstable? *Phys. Fluids* **16** (7), 2154–2157.

Morse, P. M. & Feshbach, H. 1953 *Methods of Theoretical Physics*. McGraw-Hill Book Company.

Nicholson, D. R. 1975 Parametric instabilities in inhomogeneous plasma. PhD thesis, Department of Physics, University of California, Berkely, CA.

Rayleigh, Lord 1896 *Theory of Sound*, 2nd edn., vol. 2. Macmillan and Co.

Roche, J. S., Grand, N. Le, Brunet, P., Lebon, L. & Limat, L. 2006 Perturbations on a liquid curtain near break-up: wakes and free edges. *Phys. Fluids* **18** (8), doi:10.1063/1.2238867.

Rosenbluth, M. N., White, R. B. & Liu, C. S. 1973 Temporal evolution of a three-wave parametric instability. *Phys. Rev. Lett.* **31**, 1190–1193.

Schmid, P. J. & Henningson, D. S. 2001 *Stability and Transition in Shear Flows*. Springer.

Seeley, R. T. 1966 *An Introduction to Fourier Series and Integrals*. W.A. Benjamin.

Squire, H. B. 1953 Investigation of the instability of a moving liquid film. *Brit. J. Appl. Phys.* **4**, 167–169.

Sturrock, P. A. 1958 Kinematics of growing waves. *Phys. Rev.* **112** (5), 1488–1503.

Taylor, G. I. 1959 The dynamics of thin sheets of fluid. Part II. Waves on fluid sheets. *Proc. R. Soc. Lond.* A **253**, 296–312.